Quark- and gluon-jet emission from primordial black holes: The instantaneous spectra

Jane H. MacGibbon*
Institute of Astronomy, University of Cambridge, Cambridge, CB3 0HA, England

B. R. Webber
Cavendish Laboratory, University of Cambridge, Cambridge CB3 0HA, England
(Received 29 December 1989)

We investigate the emission of quark and gluon jets from black holes with temperatures of 0.02–100 GeV, by convolving the Hawking emission formulas with a Monte Carlo QCD jet code. Jet emission may be astrophysically important particularly if black holes form from initial density perturbations in the early Universe. We find that the total emission differs dramatically from previous calculations and is dominated by the jet fragmentation products. The spectra have a significant component at energies well below the black-hole temperature, arising from the decays.

I. INTRODUCTION

Since Hawking first[1,2] described the quantum evaporation of black holes in 1974, a number of authors (see, for example, Refs. 3–6) have suggested that the emission from black holes created in the early Universe could produce observable astrophysical consequences. Such black holes may have formed, for example, from initial density perturbations or as a result of a phase transition (for a review see Ref. 5). These are the only holes small enough for quantum emission effects to be important. Limits on the present density of primordial black holes (PBH's) imply that only a minute fraction of the Universe's mass could have gone into PBH's. This in turn places important constraints on early-Universe models.[7] Thus even the nonexistence of PBH's would provide useful cosmological information.

If the PBH's formed from a scale-invariant Zel'dovich-Harrison spectrum of initial density perturbations in the radiation-dominated era, their emission may[8] explain, or contribute significantly to, the cosmic-ray γ-ray spectrum between 50 and 600 MeV and the cosmic-ray electron and positron spectra around 100 MeV. Strikingly, all upper limits on the present PBH density from the γ-ray, e^+, e^-, and $\bar{p}$ cosmic-ray data are roughly the same value[8] (about 10^{-8} in units of the critical density), provided that PBH's cluster to the same degree as the other matter in the Galactic halo. In this scenario, Planck-mass relics of the holes that have evaporated by today could also contribute substantially to the dark matter.[9] Alternatively, emission from PBH's with a less natural initial mass spectrum may explain other astrophysical anomalies, such as the 0.6–10 MeV shoulder in the γ-ray spectrum.[8] Thus it is important to study the generation of particles by PBH's as carefully as possible.

If PBH's formed in the early Universe, the initial emission from a hole which is just expiring today peaks at about 100 MeV. (If the PBH's formed from a Zel'dovich-Harrison spectrum, these $M_* \simeq 4-6\times10^{14}$ g holes are also the most numerous today.[7]) This is close to the QCD quark-hadron transition scale, $\Lambda_{\rm QH} \simeq 250-300$ MeV. However, all previous calculations of black-hole emissions have not included particle decays nor QCD emissions. In fact, because of the huge increase in the degrees of freedom for quarks and gluons, and the large number of final particles created by the decay of each quark or gluon, the quark and gluon emission dominates the black-hole evaporation above this temperature. Since a hole's lifetime is proportional to M_i^3 where M_i is the initial mass of the hole, the quarks and gluons should also have a significant effect on the radiation produced by a distribution of PBH's over the history of the Universe.

Previous approaches[3,10] to the problem also assumed that any particle species is emitted with a blackbody spectrum once the black-hole temperature exceeds the relevant rest mass. This was applied as well to particles with composite structure. In contrast, in this paper, we adopt the more conventional particle-physics view that a black hole emits only those particles which appear elementary on the scale of the radiated energy and the dimensions of the black hole at a given temperature. The evaporated particles then form into composite particles after emission. Thus, at temperatures above $\Lambda_{\rm QH}$, we envisage the black hole emitting relativistic quark and gluon jets which subsequently fragment into the stable photons, leptons, and hadrons (i.e., neutrinos, electrons, positrons, protons, and antiprotons). Since the pion rest masses are smaller than the effective quark masses, however, pions should be directly emitted at the energies below $\Lambda_{\rm QH}$. This is consistent with our current approach to high-energy accelerator interactions. In fact, we show later that the emitted quarks and gluons resemble those produced in e^+e^- collider events and hence should decay in the same way into final colorless hadronic states. So, to calculate the final emission spectra, we numerically convolve the Hawking emission formulas with a Monte Carlo QCD jet code which was written to describe jet fragmentation and clustering in collider events.

The spectra that we generate are very different from

the simple direct emission. Most of the final quark and gluon products have energies well below the energy of the initial particle—they extend all the way down to the rest mass of the decay particle. Together with large number of quark and gluon degrees of freedom and decay states, this produces convolved spectra which resemble those produced in $e^{\pm}$ annihilation events rather than the initial Hawking distribution. The number of jet-produced leptons and photons far exceeds the number of directly emitted leptons; the only protons and antiprotons emitted are jet products, since the proton rest mass is much greater than Λ_{QH}. Because of these differences, many assumptions made by previous authors investigating the cosmological consequences may no longer be valid. In particular, the cosmic-ray limits on the present PBH density were originally derived using the nonjet emission from the M_* holes.[4] (Our discussion on the cosmic-ray limits in the second paragraph of this section, however, is based on the values derived using our results.[8]) Also all $p\bar{p}$ were assumed to be directly emitted.[3,10] Using our results, one now also finds[8] that the bursts generated in the ultimate stages of PBH evaporation are practically undetectable.

In this paper, we present the instantaneous black-hole emission for temperatures of 0.02–100 GeV: in Sec. II, we review the primary Hawking emission; in Sec. III, we discuss quark and gluon emission and the characteristics of jet decay; in Sec. IV, we describe our numerical method for generating the final emission spectra; and in Sec. V, we discuss our results in detail. Subsequent papers discuss the lifetime emission from an individual black hole,[11] the emission from a background on PBH's (Ref. 12), the astrophysical consequences of such emission[8] and the modulation of the spectra by astrophysical interactions.

We also note that we restrict our list of emitted particles to just the experimentally verified species—we have not included graviton and Higgs-boson emission, etc., and have only considered three lepton families. The one exception is our inclusion of the top quark which is required by the Weinberger-Glashow-Salam theory to complete the "three family" symmetry. Although the effect of including the nonestablished particles is discussed in the text, the emission of any new species (except perhaps massless "shadow matter" states) will have a negligible effect at the energies which interest us.

II. HAWKING RADIATION

Hawking[1,2] considered an object collapsing to form a black hole. Using the usual quantum-mechanical wave equations and replacing a precollapse Minkowski metric by a postcollapse classical curved space-time metric, he found that there can be a net increase in the number of particles in the outgoing wave modes. Taking an ingoing vacuum solution, an observer at $\mathcal{I}^+$ (the positive "null" infinity of space-time) no longer sees a vacuum outgoing state but a quasi-Planckian flux evaporating off the hole. For massless particles at high energies, this is analogous to the thermal emission from a hot body with a temperature of $h\kappa/2\pi ck$ where κ is the surface gravity of the black hole. It is not surprising that the incoming vacuum state no longer corresponds to an outgoing vacuum state since the quantum modes are severely disrupted as they propagate through the object's interior. The argument essentially applies to all types of incoming fields and does not depend on the details of the collapse. Heuristically,[13] the particles could be thought of as quantum tunnelling through the event horizon whose thickness of the gravitational potential barrier $\propto\kappa$. Alternatively,[14] we could say that the gravitational field is spontaneously creating virtual particle pairs just outside the event horizon. Strong gravitational tidal forces prevent annihilation if λ, the wavelength of the virtual pair or the distance the particles travel apart, is of the order of the size of the hole $\propto\kappa^{-1}$. The classically forbidden negative-energy particle then tunnels through the event horizon to the region inside the hole where it can exist as a real particle and the positive-energy particle escapes to infinity as the observed "thermal emission."

A black hole with angular velocity Ω and electric potential Φ emits particles with total energy between $(Q, Q+dQ)$ at a rate

$$d\dot{N}=\frac{\Gamma_s dQ}{2\pi\hbar}\left[\exp\left[\frac{Q-n\hbar\Omega-q\Phi}{\hbar\kappa/2\pi c}\right]-(-1)^{2s}\right]^{-1} \quad (1)$$

per degree of particle freedom. Here s is the particle spin, $n\hbar$ is the axial quantum number or angular momentum and q is the particle charge. Γ_s is the dimensionless absorption probability for the emitted species. In general, Γ_s is a function of Q, Ω, Φ, and κ, together with the internal degrees of freedom and rest mass of the particle. Γ_s varies as Q^2 at high energies for massless or relativistic particles.

If $\Omega=\Phi=0$, Eq. (1) mimics blackbody emission and we can define a black-hole temperature of $kT=\hbar\kappa/2\pi c$. If M is the mass of the black hole, then $\kappa=c^4/4GM$ for $\Omega=\Phi=0$ and we have

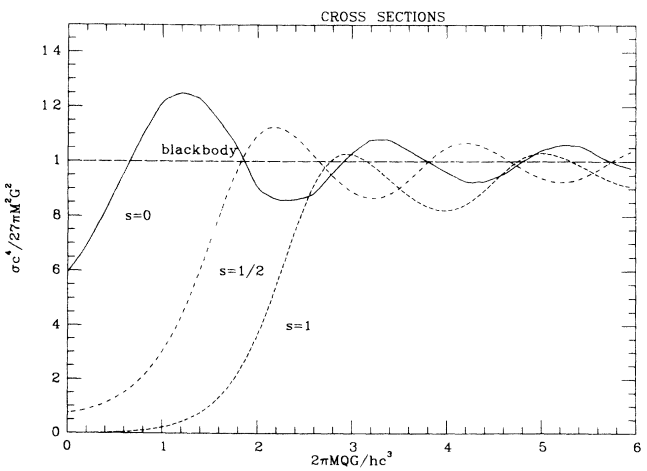

FIG. 1. Absorption cross section $\sigma\propto\Gamma/Q^2$ as a function of $MQG/\hbar c^3$. The dashed line represents the geometric optics cross section $27\pi M^2G^2/c^4$.

$$kT=\frac{\hbar c^3}{8\pi GM}=1.06\left[\frac{M}{10^{13}\text{ g}}\right]^{-1}\text{ GeV}\ . \tag{2}$$

A solar mass hole ($M_\odot\simeq 2\times 10^{33}$ g) has a temperature of about 10^{-3} K while a 6×10^{14} g hole has a temperature of 20 MeV. If $\Gamma_s\propto Q^2$, Eq. (1) peaks at $Q=2.22kT$ for nonintegral s and $Q=1.59kT$ for integral s. A hole should emit all particles whose rest masses are less than or of the order of T. Photons and massless neutrinos (or neutrinos with negligible rest masses) are emitted in substantial numbers at all temperatures. Furthermore, since the exponentially damped tail of the emission extends to $Q=\infty$, a nonzero contribution from any massive species is always present. The evaporation of massive particles, however, only becomes significant once the peak in the energy distribution reaches the particle rest mass. One can also show[15] that a black hole can act as a source of any massless gauge field, in particular the SU(3) color gauge group, and that it will conserve the associated quantum numbers. Thus, if the temperature is greater than a few hundred MeV, strongly interacting particles should also be emitted.

As the net outflow of energy decreases the mass of the black hole, the hole can be regarded as a series of stationary states with calculable emission rates. $M_\odot$ holes lose negligible mass over the lifetime of the Universe. $M\le M_*\simeq 6\times 10^{14}$ g holes, which may have formed in the early Universe, would have evaporated completely by today. (We define M_* to be the mass of a hole whose lifetime equals the age of the Universe. A new calculation of M_* as a function of the cosmological density and the Hubble constant and including nonrelativistic corrections is presented in Ref. 11.) Although Eq. (1) holds throughout the hole's lifetime, it breaks down when $M\to m_{\rm Pl}\simeq 2.18\times 10^{-5}$ g, the Planck mass. At $m_{\rm Pl}$, the space-time curvature at the event horizon is of the order of the quantum fluctuations in the metric. Because the hole's evolution rate is comparable with the time light takes to cross the hole, the quasistationary approach also breaks down $M\to m_{\rm Pl}$.

A. Absorption probabilities and cross sections

For general Q and $\Omega=\Phi=0$, the scattering matrix for incoming planar modes can be expanded in spherical harmonics to show[6,16] that $\Gamma s_s(M,Q)=Q^2\sigma_s(M,Q)/\pi\hbar^2c^2=8.16\times 10^{26}Q^2\sigma_s(M,Q)$ where σ_s is the absorption cross section in cm^2 and Q is in GeV. When a massless particle scatters off a nonrotating, uncharged hole, the low-energy ($GMQ/\hbar c^3\ll 1$) analytic form of Γ_s, averaged over all orientations of the hole with respect to the spheroidal harmonic and angular momentum quantum numbers of the incoming field, is[6,17]

$$\Gamma_s(M,Q)\underset{Q\to 0}{\sim}\begin{cases}16G^2M^2Q^2/\hbar^2c^6=2.26\times 10^{-2}\left[\dfrac{M}{10^{13}\text{ g}}\right]^2Q^2, & s=0\ ,\\ 2G^2M^2Q^2/\hbar^2c^6=2.83\times 10^{-3}\left[\dfrac{M}{10^{13}\text{ g}}\right]^2Q^2, & s=\frac{1}{2}\ ,\\ 64G^4M^4Q^4/3\hbar^4c^{12}=4.26\times 10^{-5}\left[\dfrac{M}{10^{13}\text{ g}}\right]^4Q^4, & s=1\ ,\\ 256G^6M^6Q^6/45\hbar^6c^{18}=1.61\times 10^{-8}\left[\dfrac{M}{10^{13}\text{ g}}\right]^6Q^6, & s=2\ .\end{cases} \tag{3}$$

At high energies, σ_s for each species approaches the geometric optics limit, $\sigma_g=27\pi G^2M^2/c^4$. Thus

$$\Gamma_s(M,Q)\underset{Q\to\infty}{\sim}\frac{27G^2M^2Q^2}{\hbar^2c^6}=3.82\times 10^{-2}\left[\frac{M}{10^{13}\text{ g}}\right]^2\left[\frac{Q}{\text{GeV}}\right]^2\ . \tag{4}$$

At low energies, σ_s decreases and remains finite for $s=\frac{1}{2}$ and $s=0$ but approaches zero for the other bosons. For relativistic or massless particles and $\Omega=0$, Γ_s can be regarded as a function of MQ. The exact form of Γ_s, however, must be calculated numerically. Figure 1 shows σ_s for $s=0$, $\frac{1}{2}$, and 1. The deviations from the low-energy limits (3) are already of the order of 50% for $GMQ/\hbar c^3=0.05$. The approach to the high-energy geometric limit is not monotonic. Instead the curves oscillate about the high-energy limit as higher angular modes become significant. The σ_s behavior is analogous to the s-dependent diffraction patterns seen in the (true) thermal emission and absorption by a blackbody of a particle whose wavelengths are comparable to the dimensions of the blackbody.

Between the low-energy and high-energy limits, the $\sigma_{s=1}$ curve lags behind $\sigma_{s=1/2}$. This shows up in the "averaged" cross sections

$$\bar{\sigma}_s=\frac{\int\sigma_s(M,Q)dQ}{\int dE}=\begin{cases}56.7G^2M^2/c^4=3.21\times10^{-29}\left[\dfrac{M}{10^{13}\text{ g}}\right]^2\text{cm}^2, & s=\frac{1}{2}\ ,\\ 20.4G^2M^2/c^4=1.16\times10^{-29}\left[\dfrac{M}{10^{13}\text{ g}}\right]^2\text{cm}^2, & s=1\ ,\\ 2.33G^2M^2/c^4=1.32\times10^{-30}\left[\dfrac{M}{10^{13}\text{ g}}\right]^2\text{cm}^2, & s=2\end{cases}\tag{5}$$

and hence in the greater total flux and power per $s=\frac{1}{2}$ helicity state. It also accounts for the fact that the flux and power spectra peak at lower energies for $s=\frac{1}{2}$ than for $s=1$. The peak energies however are higher, and the spectra at all Q are lower, than those for a blackbody with an energy-independent cross section of $27\pi G^2M^2/c^4$.

For massive particles, σ_s still approaches σ_g as $Q\to\infty$. For nonrelativistic fermions with rest energy μ and total energy Q, we have

$$\Gamma_s(M,Q)=\frac{\sigma_s(Q,M,\mu)}{\pi\hbar^2c^2}(Q^2-\mu^2)$$
$$=8.06\times10^{27}\left[\frac{\sigma_s(Q,M,\mu)}{\text{cm}^2}\right](Q^2-\mu^2)\ .\tag{6}$$

Γ_s is no longer solely a function of MQ. Since σ_s diverges as $v^{-2}=[1-(\mu/Q)^2]^{-1}$ in the low-momentum limit, $\Gamma_s(M,Q)$ remains finite and a function of M as $Q\to\mu$. For $GM\mu/\hbar c^3\lesssim0.4$ or $(M/10^{13}\text{ g})(\mu/\text{GeV})\lesssim10$, Γ_s differs from its relativistic value only noticeably for $Q\lesssim2\mu$. $\Gamma_{s=1/2}(M,Q)$ at $Q=\mu$ remains at least 50% of the relativistic value. Since Q must be greater than or equal to μ to emit the particle, the emission spectrum is cut off below $Q=\mu$. In general, this cutoff is more important when we calculate the total emission rate of a massive particle than the associated decrease in Γ_s.

B. Effects of charge and angular momentum

If J and q' are the nonzero angular momentum and electric charge of the black hole, then $\Omega=c^4J/2G^2M^3$ and $\Phi=c^2q'/GM$ for the unique Kerr-Newman[18–20] (stationary axisymmetric) generalization of the Schwarzschild metric to include charge and angular momentum. The generalized temperature is[21]

$$kT=\frac{2\hbar GM}{c\mathcal{A}}\left[1-\frac{c^2J^2}{G^2M^4}-\frac{q'^2}{GM^2}\right]^{1/2},\tag{7}$$

where $\mathcal{A}$ is the surface area of the black-hole horizon. If $\Omega=\Phi=0$, then $\mathcal{A}=16\pi G^2M^2c^{-4}$. For nonzero Ω or Φ, $\mathcal{A}$ is a function of J and q'. Even for $\Phi=0$, Γ_s is sensitive,[22] to the order of a few percent, to the combined effect of the electrostatic attraction between charged emitted particles and their antiparticles and the fluctuation in the hole's charge due to the stochastic emission of charged particles. Because of electrostatic repulsion, Eq. (1) implies that a hole with built-up charge preferentially emits a like-charged particle. Numerically one finds[22] that the electrostatic attraction between particles and antiparticles of charge e, together with the charge fluctuation, decreases the average emitted flux and power by $<5\%$ when compared with otherwise-similar uncharged particles. Since the quark electric charge is either $\pm e/3$ or $\pm2e/3$, the effect on quark emission rates should be smaller.

Looking at Eq. (1), we also see that an $\Omega\neq0$ black hole tends to emit particles whose angular momentum is aligned with that of the hole. Equation (1) implies, as a rough estimate, that $\dot{M}/M\sim\dot{J}/J$ when $\Phi=0$. Page, however, has shown conclusively[23] that the angular momentum of the hole is emitted several times faster than the mass. The initial spin diminishes to almost zero before most mass is given up. The emitted power also increases with angular momentum. For a given M, the increase may be up to 1 order of magnitude for neutrinos, 2 orders for photons, and 4 orders for gravitons. The lifetime of a black hole with the maximal initial rotation, $J=GM^2/c$, is decreased by about 50–60%, depending on the emitted species. If a nonrotating 5×10^{14} g hole, created in the early Universe, just expires today, a 7×10^{14} g black hole created with the maximal rotation also just expires today. These corrections are not of immense consequence, given the uncertainty in our knowledge of the age of the Universe.

In view of our remarks, we shall assume in this paper an uncharged, nonrotating Schwarzschild black-hole configuration, i.e., $\Omega=\Phi=0$. We also neglect the effect on Γ_s of the particle's charge or nonrelativistic energy. The latter is justified for $e^{\pm}$ since the flux and power from an $M\lesssim M_*$ black hole peak well above 10^2m_e: the nonrelativistic corrections only apply to a tiny fraction of the spectrum. Directly emitted neutrinos with rest mass $m_\nu\lesssim10^2m_e$ are also unaffected. $M\simeq M_*$ holes today are emitting muons whose energies are predominantly $m_\mu\lesssim Q\ll2m_\mu$, where $m_\mu\simeq0.106$ GeV. The nonrelativistic flux is at least 55% of the relativistic value at the same Q. As M decreases and the average Q becomes $\gtrsim2m_\mu$, the deviation becomes less relevant. More importantly, the holes also start to emit hadrons or their constituents. These particles, with their huge increase in internal degrees of freedom, dominate the directly produced leptons. The uncertainty in the form of the cutoff in hadron production in any particle model around the quark-hadron transition, Λ_{QH} is at least comparable with the nonrelativistic corrections to Γ_s. To determine M_* more exactly, this must be taken into account,[11] along with possible contributions from heavier particles.

C. Flux and power spectra of primary species

The emitted[6,22,24] primary $s=\frac{1}{2}$ and $s=1$ flux, $d\dot{N}$, and power, $Qd\dot{N}$, are shown in Fig. 2 together with the thermal radiation from a blackbody with a cross section of $\sigma=27\pi G^2M^2/c^4$ and dimensions much greater than the radiation wavelength. At high energies the spectra approach the blackbody emission spectra. At low energies, they drop significantly below since Γ_s falls off more steeply than $27G^2M^2Q^2/\hbar^2c^6$. This spin-dependent low-energy effect, however, is analogous to the optical phenomenon of resonant scattering off a spherical body whose dimensions are comparable with the incident wavelength or the thermal emission from a body whose dimensions are comparable with the radiation wavelength. The small bumps in the neutrino flux and power spectra at about $GMQ/\hbar c^3\simeq 0.4$, and the photon spectra at $GMQ/\hbar c^3\simeq 0.4$ and $GMQ/\hbar c^3\simeq 0.5$, respectively, come from the higher-order $l>s$ angular modes in $\Gamma_{s,p}$.

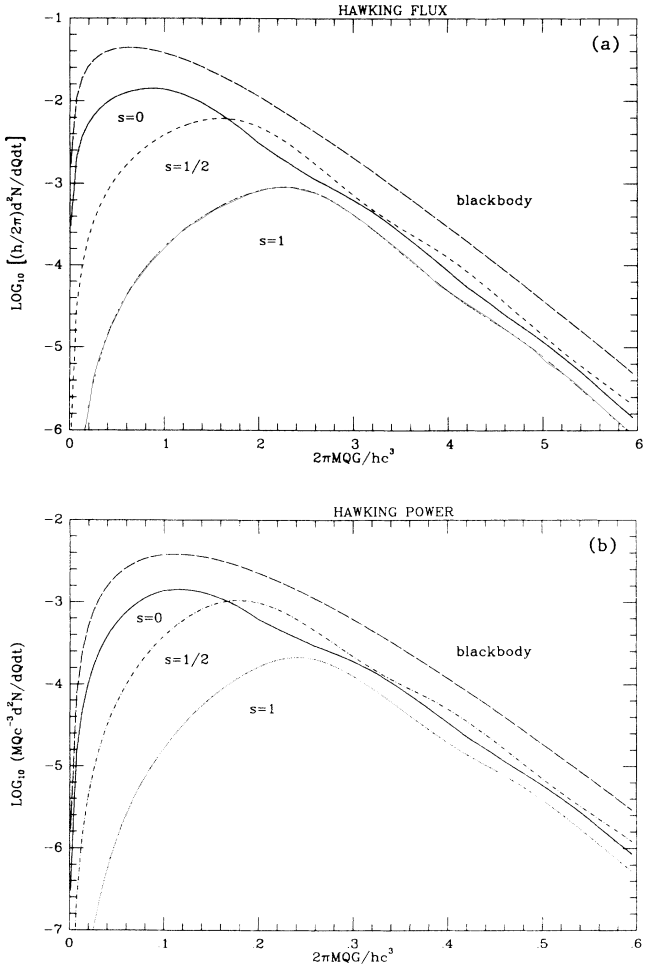

FIG. 2. (a) The primary pion, $e^{\pm}$, and photon Hawking flux as a function of $MQG/\hbar c^3$. The dashed line represents the emission from a blackbody with a constant cross section of $27\pi M^2G^2/c^4$ with arbitrary normalization. (b) The primary pion, $e^{\pm}$, and photon power. The dashed line again represents the emission from a blackbody with a cross section of $27\pi M^2G^2/c^4$.

The flux of $s=\frac{1}{2}$ electrons and positrons with two helicity states each, and $s=1$ photons with two polarizations, peaks at[24]

$$\begin{aligned} &MQ_{s=1/2}=4.26\times10^{13}\ \text{g GeV}\ ,\\ &\frac{d\dot{N}}{dQ}=9.39\times10^{21}\ \text{GeV}^{-1}\text{sec}^{-1},\quad e^+e^-\ ,\\ &MQ_{s=1}=6.12\times10^{13}\ \text{g GeV}\ ,\\ &\frac{d\dot{N}}{dQ}=1.38\times10^{21}\ \text{GeV}^{-1}\text{sec}^{-1},\quad \gamma\ , \end{aligned} \tag{8}$$

respectively. Here we have summed over all helicity states. The power spectra peak at

$$\begin{aligned} &MQ_{s=1/2}=4.74\times10^{13}\ \text{g GeV}\ ,\\ &Q\frac{d\dot{N}}{dQ}=\frac{4.25\times10^{22}}{M/10^{13}\ \text{g}}\ \text{sec}^{-1},\quad e^+e^-\ ,\\ &MQ_{s=1}=6.38\times10^{13}\ \text{g GeV}\ ,\\ &Q\frac{d\dot{N}}{dQ}=\frac{8.62\times10^{21}}{M/10^{13}\ \text{g}}\ \text{sec}^{-1},\quad \gamma\ . \end{aligned} \tag{9}$$

The $s=1$ peaks occur at higher MQ since Γ_s cuts off more steeply as $MQ\rightarrow 0$. The neutrino values were unavailable.

Summing over all emitted energies, the integrated flux and power contributions from each helicity or polarization state are

$$\begin{aligned} &\dot{N}=\frac{9.81\times10^{21}}{M/10^{13}\ \text{g}}\ \text{sec}^{-1}\ ,\\ &P=\int Q\frac{d\dot{N}}{dQ}dQ=\frac{4.39\times10^{22}}{(M/10^{13}\ \text{g})^2}\ \text{GeV sec}^{-1},\quad \nu\bar{\nu}\ ,\\ &\dot{N}=\frac{9.61\times10^{21}}{M/10^{13}\ \text{g}}\ \text{sec}^{-1}\ ,\\ &P=\frac{4.26\times10^{22}}{(M/10^{13}\ \text{g})^2}\ \text{GeV sec}^{-1},\quad e^+e^-\ ,\\ &\dot{N}=\frac{2.99\times10^{21}}{M/10^{13}\ \text{g}}\ \text{sec}^{-1}\ ,\\ &P=\frac{1.81\times10^{22}}{(M/10^{13}\ \text{g})^2}\ \text{GeV sec}^{-1},\quad \gamma\ . \end{aligned} \tag{10}$$

Since the emission is a quasithermal process, $P\propto\mathcal{A}T^{-4}\propto M^{-2}$. In the relativistic or massless limit, Elster and Simkins[25–27] find the integrated flux and power per $s=0$ state to be

$$\begin{aligned} &\dot{N}=\frac{2.69\times10^{22}}{M/10^{13}\ \text{g}}\ \text{sec}^{-1}\ ,\\ &P=\frac{7.80\times10^{22}}{(M/10^{13}\ \text{g})^2}\ \text{GeV sec}^{-1} \end{aligned} \tag{11}$$

for uncharged particles. The average particle energy is $\bar{E}_{s=0}=2.81kT$. (In this paper, we assume that the $s=0$ power peaks at $\bar{E}_{s=0}$. The error in this assumption is less than 5%.)

For an $M \gg 10^{17}$ g black hole, which is emitting only massless particles (three kinds of neutrinos and the photon), the total flux and power are

$$\sum \dot{N} = \frac{6.48 \times 10^{22}}{M/10^{13}\ \text{g}}\ \text{sec}^{-1}\ ,$$
$$\sum P = \frac{3.00 \times 10^{23}}{(M/10^{13}\ \text{g})^2}\ \text{GeV sec}^{-1}\ . \tag{12}$$

91% of the total flux is neutrinos and 9% photons. 88% of the total power is carried by neutrinos and 12% by photons. If we amend the particle list to include $s=2$ particles—for example, the graviton with two helicity states—each new $s=2$ state contributes[6]

$$\dot{N} = \frac{0.220 \times 10^{21}}{M/10^{13}\ \text{g}}\ \text{sec}^{-1}\ ,$$
$$P = \frac{0.206 \times 10^{22}}{(M/10^{13}\ \text{g})^2}\ \text{GeV sec}^{-1}\ . \tag{13}$$

In summary, the flux and power are highly spin dependent. The emission process is more strongly coupled to particles with smaller s. This is also true for (classical) "superradiance" from a black hole[28] and for nuclear scattering.[29] Intuitively, it is not surprising since one would expect it to be harder to scatter particles with higher intrinsic spin. Since one can show[6] that Γ_s involves terms to the power $2s+1$, at least in the low-energy approximation, rough estimates of the contributions from other species can be obtained by plotting the logarithms of the contributions per helicity or polarization as a function of s and then interpolating. This gives reasonable accuracy without recourse to the extraordinary computational time required for the full determination of Γ_s.

A $10^{14}\ \text{g} < M \ll 10^{17}$ g black hole should also emit relativistic electrons and positrons. Assuming the hole emits only the experimentally established particles (three kinds of neutrinos, $e^{\pm}$ and photons), the total flux and power are then

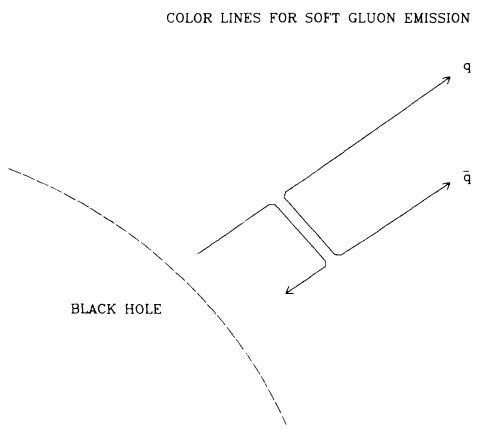

FIG. 3. Color lines for the emission of a soft gluon by an evaporated quark close to the black hole.

$$\dot{N} = \frac{1.03 \times 10^{23}}{M/10^{13}\ \text{g}}\ \text{sec}^{-1}\ ,$$
$$P = \frac{4.70 \times 10^{23}}{(M/10^{13}\ \text{g})^2}\ \text{GeV sec}^{-1}\ . \tag{14}$$

As the rest masses of further $s=\frac{1}{2}$ particles are surpassed, the flux and power from each new degree of freedom are approximately given by Eq. (10). Since the flux and power spectra peak at about $5T$, most of the particles are relativistic once T reaches the particle rest energy, disregarding the effect of particle charge. Thus the nonrelativistic corrections discussed earlier need only be applied when the flux and power peak around the particle rest mass.

To add in the new states, we note that the $\mu^{\pm}$ and $\tau^{\pm}$ leptons have two helicity states per particle or antiparticle. Each $s=\frac{1}{2}$ quark flavor has 12 degrees of freedom—three color degrees of freedom and two helicity states per particle or antiparticle. If the $s=1$ QCD gauge bosons, the gluons, are emitted once T reaches their effective confinement mass, $m_g \simeq 600$–700 MeV, the relevant contributions per $s=1$ degree of freedom are multiplied by 16 for the eight color degrees of freedom and the two helicity states. (We assume the gluon contribution per degree of freedom approximately equals the photon contribution.) The $s=0$ pions, whose contributions per helicity state are 3–4 times the $s=\frac{1}{2}$ contribution, can exist in three states: π^0, π^+, and π^-, with $m_{\pi^0} \simeq 135$ MeV and $m_{\pi^{\pm}} \simeq 140$ MeV. Although an M_* black hole evaporates for most of its lifetime at $T \simeq 0.02$ GeV, the huge increase in the degrees of freedom and the number of fragmentation products per quark and gluon implies that the emission from the holes with higher temperatures may be required to calculate the present particle backgrounds produced by PBH evaporation over the lifetime of the Universe.

In the most natural scenario, a black hole should fundamentally emit those particles which appear elementary on the scale of the radiated energy and the dimensions of the hole (see Sec. III A), rather than particles with composite structure. The particles then combine to form composite particles after emission. In particular, when Q exceeds the effective quark and gluon confinement masses, quarks and gluons rather than composite hadrons should be fundamentally emitted. Since pions are notably lighter than the effective quark masses, $m_q \gtrsim 300$ MeV, primary pions should be directly emitted at the energies below the lowest quark mass. This is consistent with our current approach to high-energy accelerator interactions: above certain "confinement" energy regimes, the interactions are regarded as involving the substructure of the particles. If further higher energy confinement thresholds are discovered, a black hole at the higher temperatures should radiate the elementary states associated with the new substructure. For a standard Glashow-Weinberg-Salam model with 40–100 elementary modes between 0.3 and 100 GeV, the emitted flux and power are roughly

$$\frac{dN}{d\tilde{t}} \simeq \frac{10^{-2}}{\tilde{M}}\ ,\quad \tilde{P} = \frac{10^{-3}}{\tilde{M}^2}\ , \tag{15}$$

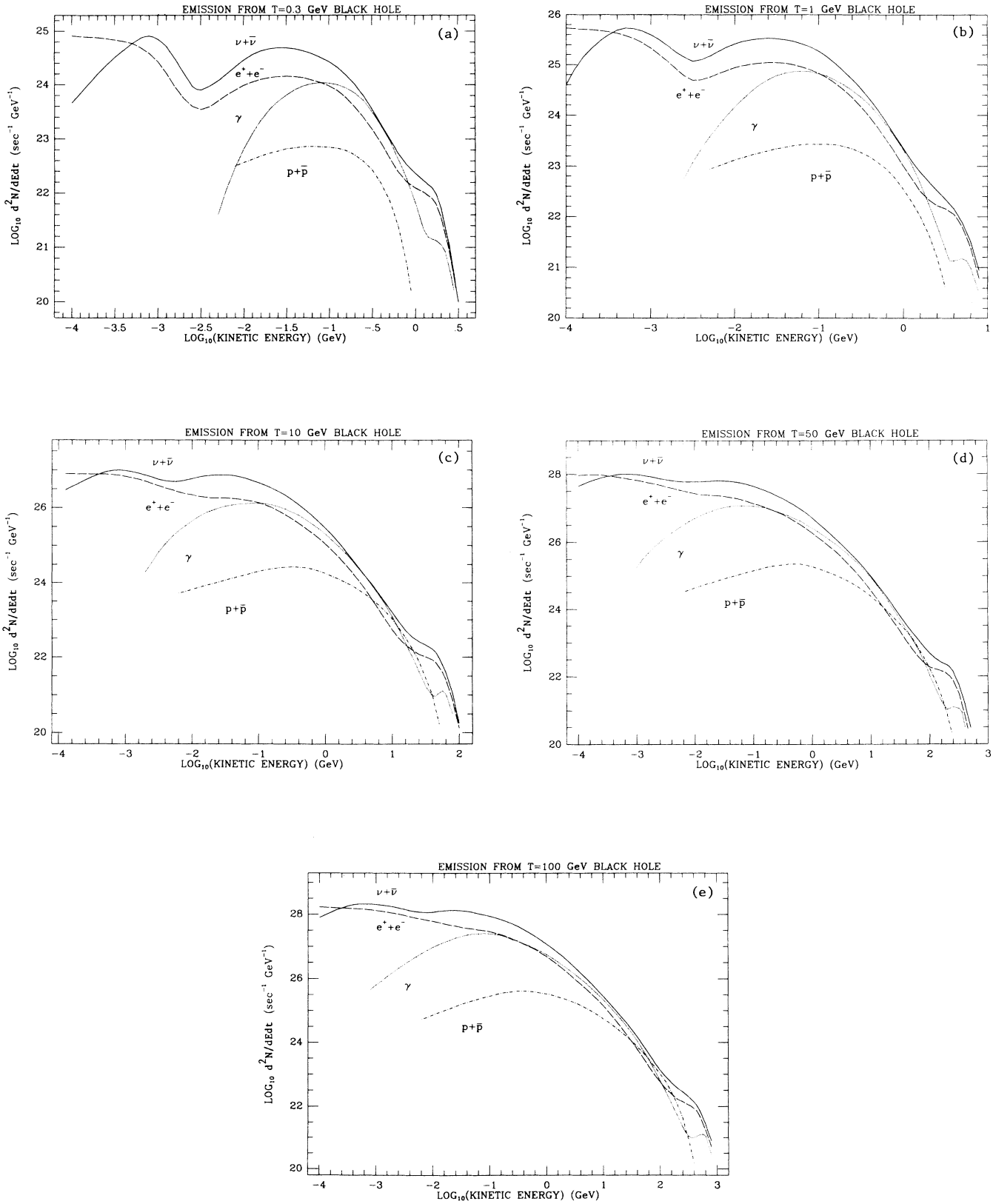

FIG. 4. The flux from (a) $T=0.3$ GeV black hole, (b) a $T=1$ GeV black hole, (c) a $T=10$ GeV black hole, (d) a $T=50$ GeV black hole, (e) a $T=100$ GeV black hole.

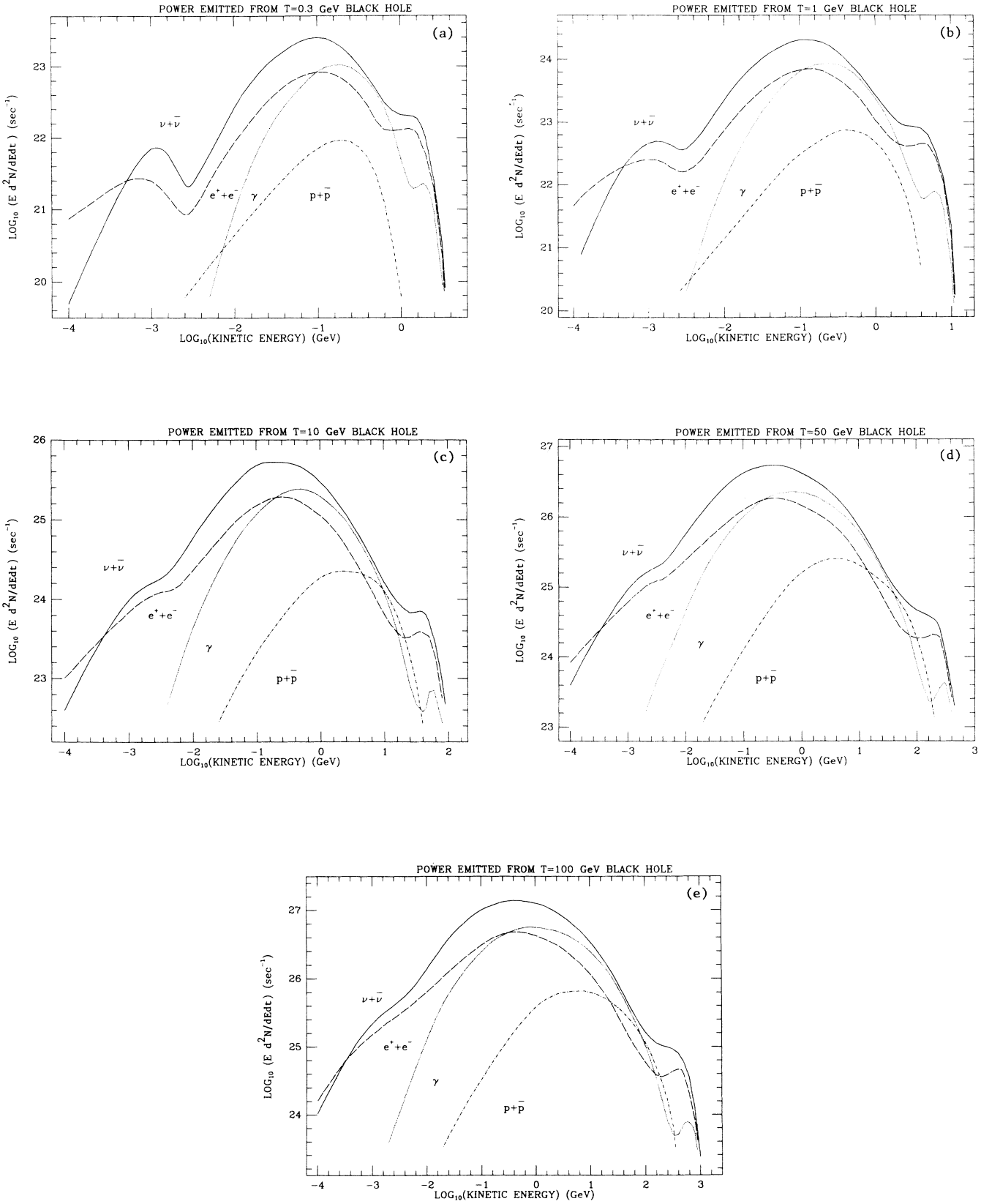

FIG. 5. The power emitted by (a) a $T=0.3$ GeV black hole, (b) a $T=1$ GeV black hole, (c) a $T=10$ GeV black hole, (d) a $T=50$ GeV black hole, (e) a $T=100$ GeV black hole.

summing over all species, where the tilde denotes dimensionless Planck units, i.e., $\hbar=c=G=k=1$.

In general, massive particles other than $p\bar{p}$ and $e^{\pm}$ are unstable on astrophysical time scales. (In particular, if τ_n' is the neutron's lifetime, $\tau_n' \gtrsim 10^{17}$ sec only if $E \gtrsim 3\times 10^{14}$ GeV; for $E \lesssim 100$ GeV, $\tau_n' \lesssim 1$ day.) Thus Eq. (1) must be convolved with the decay functions of the primary particles. If $dg_{jX}(Q,E)/dE$ is the relative number of particles X with energy E produced by particle j with energy Q, the instantaneous flux of species X from a black hole is

$$\frac{d\dot{N}_X}{dE}=\sum_j \int_{Q=E}^{Q=\infty} \frac{\Gamma_j(Q,T)}{2\pi\hbar}\left[\exp\frac{Q}{kT}-(-1)^{2s_j}\right]^{-1} \times\frac{dg_{jX}(Q,E)}{dE}dE \ . \tag{16}$$

Here we must sum over all the contributing species and their associated degrees of freedom. To normalize $dg_{jX}(Q,E)/dE$, we note that (i) $dg_{jj}(Q,E)/dE=\delta(Q-E)$ and that (ii) $\int [dg_{jX}(Q,E)/dE]dE$ = the number of X particles produced by j. All previous calculations of black-hole emissions have not included particle decays or QCD emissions.

III. QUARK- AND GLUON-JET EMISSION

A. General comments on particle emission and jets (Ref. 30)

A relativistic particle of energy Q has a de Broglie wavelength, a measure of the effective size of the interacting particle, of $\lambda_b=\hbar c/Q=0.197\times 10^{-13}(Q/\text{GeV})^{-1}$ cm. (In the nonrelativistic case, Q/c is replaced by the momentum.) The radius of the black hole is

$$r_{\rm bh}=\frac{2GM}{c^2}=1.49\times 10^{-13}\left[\frac{M}{10^{13}\ \text{g}}\right]\text{cm} =1.57\times 10^{-13}\left[\frac{T}{\text{GeV}}\right]^{-1}\text{cm} \ . \tag{17}$$

Since the flux and power peak at about $5T$, we then have

$$\lambda_b \simeq 0.04\times 10^{-13}\left[\frac{T}{\text{GeV}}\right]^{-1}\text{cm} \ll r_{\rm bh} \ , \tag{18}$$

where Q is taken to be the peak energy of the evaporated particle as measured at infinity. Hence almost all particles emitted at a given T are effectively much smaller than the hole.

If the time between the successive emissions is too small—less than the inverse of the frequency associated with λ_b—or equivalently, if the distance travelled by the particle before the hole emits another particle is less than λ_b, we would expect interactions between the particles regardless of their species. (If this did happen, we might expect a dense interacting cloud to surround the hole.) Equation (15) gives the time between successive emissions as

$$\Delta\tilde{t}\simeq 100\tilde{M}=\frac{100}{8\pi\tilde{T}}\simeq\frac{20}{\tilde{Q}}\gg\lambda_b=\frac{1}{\tilde{Q}} \ , \tag{19}$$

where $\tilde{Q}$ is the peak energy. Oliensis[30] has numerically

TABLE I. The errors in plotting $d\dot{N}/dE$ and $E\,d\dot{N}/dE$ as a function of energy E (in GeV) for $T=0.3-100$ GeV. The errors at all other energies are less than 10%.

T (GeV)		$p\bar{p}$	$e^{\pm}$	γ	$\nu\bar{\nu}$
0.3	Flux	50% for $E<0.05$ 30% for $E>0.6$	20% for $E<0.001$ 20% for $E>2$	10% for $E<0.01$ 10% for $E>2$	10% for $E<0.001$ 10% for $E>2$
	Power	20% for $E<0.025$ 20% for $E>0.6$	10% for $E<0.003$ 10% for $E>2$	20% for $E<0.025$ 20% for $E>2$	10% for $E<0.001$ 20% for $E>2$
1	Flux	25% for $E<0.025$ 20% for $E>2$	10% for $E<0.001$ 10% for $E>6$	10% for $E<0.01$ 10% for $E>6$	10% for $E<0.001$ 10% for $E>6$
	Power	30% for $E<0.025$ 20% for $E>3$	10% for $E<0.001$ 10% for $E>6$	20% for $E<0.008$ 20% for $E>6$	10% for $E<0.001$ 20% for $E>6$
10	Flux	50% for $E<0.1$ 50% for $E>10$	20% for $E<0.01$ 20% for $E>60$	20% for $E<0.01$ 20% for $E>60$	30% for $E<0.01$ 20% for $E>60$
	Power	50% for $E<0.025$ 50% for $E>10$	25% for $E<0.001$ 25% for $E>60$	25% for $E<0.01$ 25% for $E>60$	25% for $E<0.001$ 25% for $E>60$
50	Flux	50% for $E<0.1$ 50% for $E>100$	20% for $E<0.01$ 25% for $E>300$	30% for $E<0.025$ 25% for $E>300$	30% for $E<0.01$ 25% for $E>300$
	Power	50% for $E<0.1$ 25% for $E>100$	10% for $E<0.001$ 25% for $E>300$	25% for $E<0.01$ 25% for $E>300$	10% for $E<0.001$ 25% for $E>300$
100	Flux	60% for $E<0.1$ 50% for $E>100$	20% for $E<0.001$ 30% for $E>600$	50% for $E<0.01$ 30% for $E>600$	30% for $E<0.01$ 50% for $E>600$
	Power	50% for $E<0.1$ 50% for $E>200$	10% for $E<0.001$ 20% for $E>600$	20% for $E<0.01$ 20% for $E>600$	25% for $E<0.001$ 20% for $E>600$

calculated that more than 99.9% of the particles emitted over a hole's lifetime satisfy the condition $\Delta\tilde{t} > 1/\tilde{Q}$ and hence should effectively be noninteracting. Also, since $\tilde{r}_{\rm bh} \simeq \Delta\tilde{t}/50 \ll \Delta\tilde{t}$, we can assume that the emission process itself is unaffected by previously emitted particles. In summary, the particles do not interact due to short-range forces before fragmenting.

One can also show, using general arguments,[30] that high-temperature black holes emit sufficiently frequently that long-range forces (e.g., color) are unimportant to the short-range propagation of the particles, except perhaps near rest-mass thresholds. For an asymptotically free theory, both the distance between successively emitted particles and the size of the hole will be much less than $\tilde{D}_{\rm QH} = 1/\tilde{\Lambda}_{\rm QH} \simeq 10^{-13}$ cm, the scale on which the force is strong, provided $T, Q \gtrsim \Lambda_{\rm QH}$. Since T must be greater than about $\Lambda_{\rm QH}$ to emit strong particles in the first place, Δt is thus short enough that most particles can be regarded as asymptotically free at emission, i.e., there is no strong interaction between successive emissions. The emitted quarks and gluons fragment into further quarks and gluons and then cluster into the observed hadrons once they have traveled a distance $\tilde{D}_{\rm QH}$. Strictly speaking, $\tilde{D}_{\rm QH}$ should be enhanced by a Lorentz factor, Q_a/m_a, where m_a represents an averaged rest (or "effective") mass of the particles involved in the decay and Q_a is an averaged energy. $\tilde{D}_{\rm QH}$ should also be dilated by a general-relativistic factor $1/\sqrt{1-2\tilde{M}/\tilde{r}}$, where $\tilde{r}$ is the distance from the black-hole singularity.

The lifetime of the individual quarks or gluons produced in the jet before hadronization occurs is $\tau \simeq \hbar/m$ in the rest frame of the particle, where m is the effective rest mass. In the frame at rest relative to the hole, then, the particle travels a distance $D_p \simeq \hbar c Q/m^2 \simeq 5\hbar c k T/m^2$ before decaying. (We have neglected for the moment the gravitational effects on τ.) This implies, $r_{\rm bh} \lesssim D_p$ for $0.6m \lesssim T$. The possibility that a particle may travel less than $r_{\rm bh}$ before decaying should only be of consequence if it is created closer to the event horizon of the hole. However, in this case, the energy of the particle in the local frame is blueshifted by $1/\sqrt{1-2\tilde{M}/\tilde{r}}$ compared to its value at infinity and the lifetime is also increased by this amount. If the initial particle in the jet can be considered to be "evaporated" at a distance $\tilde{r}_{\rm ev} = 3\tilde{M}$ (the solution at this distance already closely approximates the solution for the particle at $r = \infty$), the blueshift is less than 1.73. At $\tilde{r} = 5\tilde{M}$, the blueshift is 1.29; at $\tilde{r} = 10\tilde{M}$, it is 1.05. Thus the gravitationally induced curvature near a hole is generally not important to jet decay. The correction required for low-momentum particles created close to a

TABLE II. Fractions of total flux, $\dot{N}_{\rm tot}$, in each species for $T = 0.3$–100 GeV. The errors shown are the statistical errors.

T (GeV)		$p\bar{p}$	$e^{\pm}$	γ	$\nu\bar{\nu}$
0.3	Flux (% of $\dot{N}_{\rm tot}$)	1.75% (±0.04%)	20.62% (±0.23%)	20.33% (±0.23%)	57.30% (±0.49%)
			$\dot{N}_{\rm tot} = 1.13(\pm 0.02) \times 10^{24}$ GeV^{-1} sec^{-1}		
	Jet products (% of $\dot{N}_{\rm tot}$)	1.75% (±0.04%)	18.24% (±0.27%)	19.89% (±0.25%)	52.69% (±0.55%)
1	Flux (% of $\dot{N}_{\rm tot}$)	1.75% (±0.03%)	20.15% (±0.14%)	20.89% (±0.15%)	57.20% (±0.31%)
			$\dot{N}_{\rm tot} = 1.05(\pm 0.01) \times 10^{25}$ GeV^{-1} sec^{-1}		
	Jet products (% of $\dot{N}_{\rm tot}$)	1.75% (±0.03%)	18.89% (±0.16%)	20.35% (±0.16%)	54.13% (±0.37%)
10	Flux (% of $\dot{N}_{\rm tot}$)	2.18% (±0.03%)	19.62% (±0.13%)	22.19% (±0.14%)	56.01% (±0.28%)
			$\dot{N}_{\rm tot} = 3.89(\pm 0.08) \times 10^{26}$ GeV^{-1} sec^{-1}		
	Jet products (% of $\dot{N}_{\rm tot}$)	2.18% (±0.03%)	19.25% (±0.13%)	22.00% (±0.20%)	44.06% (±0.29%)
50	Flux (% of $\dot{N}_{\rm tot}$)	2.30% (±0.02%)	19.64% (±0.09%)	22.09% (±0.09%)	55.97% (±0.19%)
			$\dot{N}_{\rm tot} = 4.28(\pm 0.09) \times 10^{27}$ GeV^{-1} sec^{-1}		
	Jet products (% of $\dot{N}_{\rm tot}$)	2.30% (±0.02%)	19.49% (±0.09%)	22.02% (±0.10%)	55.59% (±0.19%)
100	Flux (% of $\dot{N}_{\rm tot}$)	2.37% (±0.02%)	19.63% (±0.09%)	22.13% (±0.10%)	55.88% (±0.21%)
			$\dot{N}_{\rm tot} = 1.12(\pm 0.03) \times 10^{28}$ GeV^{-1} sec^{-1}		
	Jet products (% of $\dot{N}_{\rm tot}$)	2.37% (±0.02%)	19.50% (±0.44%)	22.07% (±0.11%)	55.59% (±0.21%)

$T \ll m$ hole is of the order of the nonrelativistic correction to Γ_s and the uncertainties in quark and gluon behavior near mass thresholds. On the scale of the strong force, the emission of the quarks or gluons appears as simultaneous production at a point if $T \gtrsim \Lambda_{QH}$ [see Eq. (9)] and will be dressed on long distances into jets analogous to those produced in e^+e^- annihilation. Since $r_{bh} \ll D_{QH}$ for $T \gtrsim \Lambda_{QH}$ and since we can regard the quarks as "free" on scales below D_{QH}, the black-hole bubble models,[31] which have the quarks trapped within a bubble surrounding the hole simply "because. . .free quarks do not exist," would seem to be contradicted by our analysis.

At very low T the long-range forces are not relevant. For $Q \simeq \Lambda_{QH}$, i.e., below the effective quark and gluon masses, low-mass bound states should be emitted, again independently on the scale of their interactions, rather than asymptotically free quarks or gluons. Thus between approximately 100 MeV and Λ_{QH}, pions will be emitted as noncomposite particles. Although the behavior of elementary particle theories near Λ_{QH} is highly uncertain, the cutoff and decrease in Γ_s near rest mass together with the huge increase in the degrees of particle freedom and multiplicity of final states for $Q \gtrsim \Lambda_{QH}$ ensure that the precise behavior near Λ_{QH} is not needed to calculate the lifetime emission from a hole or the emission from a cosmological background of black holes.

B. Further comments on jet and color emission

We can think of the jet fragmentation in the following way:[32] consider a $q\bar{q}$ pair produced close to the hole's horizon with one quark tunneling back into the hole. Because of gluon self-interactions, the color force field lines between the q and $\bar{q}$ are squeezed into a "tubelike" region between the two particles. If the tube has constant energy density per unit length, the potential energy between the particles is proportional to the distance between them. As the $q\bar{q}$ separate, the color lines stretch until there is sufficient potential energy to create another $q\bar{q}$ pair. These particles now become the end points for the color lines and the original color tube splits in two. The process continues until the kinetic energy of the final quarks and gluons is small enough that the color coupling dominates and hadronization—the clustering of particles into color-singlet states—commences.

In the laboratory frame, the opening angle between the particles in each pair decreases[33,34] with successive branching as the partons evolve nearer "on mass shell". For the timelike parton branching in e^+e^- annihilation jets, if p_1 is the four-momentum of particle 1 which fragments into particles 2 and 3 with total energies E_2 and E_3 and negligible virtual masses, the opening angle between 2 and 3 satisfies

TABLE III. Fractions of total power, P_{tot}, carried by each species for $T = 0.3-100$ GeV.

T (GeV)		$p\bar{p}$	$e^{\pm}$	γ	$\nu\bar{\nu}$
0.3	Power	10.23%	20.65%	23.09%	46.03%
	(% of P_{tot})	(±0.31%)	(±0.47%)	(±0.51%)	(±0.99%)
			$P_{tot} = 2.17(\pm 0.05) \times 10^{23}$ sec^{-1}		
	Jet products	10.23%	11.18%	21.37%	30.35%
	(% of P_{tot})	(±0.31%)	(±0.94%)	(±0.64%)	(±1.34%)
1	Power	8.79%	20.19%	24.14%	46.89%
	(% of P_{tot})	(±0.19%)	(±0.30%)	(±0.35%)	(±0.66%)
			$P_{tot} = 3.03(\pm 0.05) \times 10^{24}$ sec^{-1}		
	Jet products	8.79%	12.14%	22.20%	32.15%
	(% of P_{tot})	(±0.19%)	(±0.46%)	(±0.42%)	(±0.69%)
10	Power	11.22%	18.71%	24.73%	45.33%
	(% of P_{tot})	(±0.20%)	(±0.23%)	(±0.25%)	(±0.43%)
			$P_{tot} = 3.56(\pm 0.09) \times 10^{26}$ sec^{-1}		
	Jet products	11.22%	12.13%	23.12%	32.86%
	(% of P_{tot})	(±0.20%)	(±0.59%)	(±0.34%)	(±0.71%)
50	Power	11.36%	18.79%	24.77%	45.08%
	(% of P_{tot})	(±0.21%)	(±0.30%)	(±0.41%)	(±0.92%)
			$P_{tot} = 9.79(\pm 0.28) \times 10^{27}$ sec^{-1}		
	Jet products	11.36%	12.37%	23.26%	33.75%
	(% of P_{tot})	(±0.21%)	(±0.53%)	(±0.50%)	(±1.22%)
100	Power	11.10%	18.93%	24.70%	45.27%
	(% of P_{tot})	(±0.17%)	(±0.19%)	(±0.25%)	(±0.52%)
			$P_{tot} = 3.91(\pm 0.12) \times 10^{28}$ sec^{-1}		
	Jet products	11.10%	12.37%	23.22%	24.52%
	(% of P_{tot})	(±0.17%)	(±0.44%)	(±0.36%)	(±0.84%)

$$p_1^2 \simeq 2E_2E_3(1-\cos\theta_{23})/c^2 \ . \tag{20}$$

Since the sum of the four-momenta is conserved, $E(P_1)=E_2+E_3$. In jet computer codes, the virtuality of the initial evaporated quark must be reconstructed using Eq. (20), but[24] is of the order of Q^2. Since p_1^2 is Lorentz invariant, Eq. (20) also implies that the jets with higher center-of-mass energies are more strongly collimated, i.e., there is less dispersion of the particles around the center-of-mass axis.

Since we cannot have unconfined color or nonintegral electric charge on distances greater than $D_{\rm QH}$, the jet process requires a method of balancing the charge before the hadronization is complete. To produce a final colorless state, either we could include in the clustering phase at least one spectator quark unmatched in another decay. Or, following the example of the Drell-Yan process, we could invoke soft-gluon emission to decouple the emitted quark or gluon from the hole. In this case, the last step in the fragmentation process is the emission of a soft gluon close to the hole, which then splits into a $q\bar{q}$ pair. The color lines for the process are shown in Fig. 3. One quark balances the color charge in the jet while the other falls back into the hole, neutralizing the hole's color charge. The electric charge can also be balanced. This scenario may be superfluous, however; since the time between successive emissions is much smaller than $\tilde{t}_{\rm QH}=1/\tilde{\Lambda}_{\rm QH}$, the statistical fluctuations in the hole's color and electric charge should average to zero over $\tilde{t}_{\rm QH}$.

C. Analytic approximations to the emission spectra

Let us now consider the QCD jet fragmentation function $dg_{jh}(Q,E)/d\ \ln E$ which describes the decay of particle j with energy Q into a hadron h, which is final on beam collider time scales. Empirically, $dg_{jh}(Q,E)/d\ \ln E$ peaks at[35]

$$E'_{\rm peak} \simeq \sqrt{\mu Q/2}\ , \qquad \mu \simeq \begin{cases} 0.05(\pm 0.02)\ \text{GeV}, & \pi^{\pm}\ , \\ 0.35(+0.23,-0.12)\ \text{GeV}, & p\bar{p} \end{cases} \tag{21}$$

TABLE IV. The average numbers (multiplicities) of $p\bar{p}$, $e^{\pm}$, γ, and $\nu\bar{\nu}$ per primary emitted particle for $T=0.3$–100 GeV.

T (GeV)	$p\bar{p}$	$e^{\pm}$	γ	$\nu\bar{\nu}$
0.3	0.124 (±0.001)	1.475 (±0.002)	1.434 (±0.003)	4.043 (±0.005)
1	0.267 (±0.001)	3.098 (±0.003)	3.177 (±0.005)	8.700 (±0.010)
10	1.041 (±0.003)	9.424 (±0.013)	10.599 (±0.019)	26.762 (±0.050)
50	2.163 (±0.005)	18.467 (±0.032)	20.753 (±0.039)	52.466 (±0.097)
100	2.889 (±0.008)	23.996 (±0.055)	27.051 (±0.066)	68.15 (±0.016)

TABLE V. Average kinetic energies for $T=0.3$–100 GeV.

T (GeV)	$\bar{E}_{p\bar{p}}$ (GeV)	$\bar{E}_{e^{\pm}}$ (GeV)	$\bar{E}_{\gamma}$ (GeV)	$\bar{E}_{\nu\bar{\nu}}$ (GeV)
0.3	0.190 (±0.001)	0.192 (±0.001)	0.219 (±0.001)	0.155 (±0.001)
1	0.515 (±0.001)	0.289 (±0.001)	0.335 (±0.001)	0.238 (±0.001)
10	3.781 (±0.009)	0.872 (±0.002)	1.021 (±0.001)	0.741 (±0.001)
50	10.340 (±0.023)	2.187 (±0.009)	2.565 (±0.013)	1.843 (±0.018)
100	15.450 (±0.040)	3.367 (±0.006)	3.899 (±0.005)	2.829 (±0.012)

for relativistic energies. (This neglects, for example, neutron β decay which is relevant on astrophysical time scales.) Here $\mu \simeq m_h/3$ where m_h is the hadronic mass. Equation (21) applies provided[33] $Q \gtrsim Q_c^2/2\mu$ where Q_c is set by the typical hadronic cluster mass: $Q_c \simeq 1.5$ GeV. At low Q, phase-space limitations take over and the peak position remains almost stationary at $E'_{\rm peak} \simeq Q_c/2$. (For nonrelativistic values of E, E/c should be replaced by the hadronic momentum.)

Since the shape of the peak is roughly Gaussian,[35] we can approximate it by

$$\frac{dg_{jh}}{d\ \ln E} \propto e^{-(y-y_0)^2/2\sigma^2}\ , \tag{22}$$

where $y=\ln(E/Q)$, y_0 is the peak position, and $\sigma^2 = A\,[\ln(Q/\Lambda_{\rm QH})]^{3/2}$ is the Q-dependent width. The con-

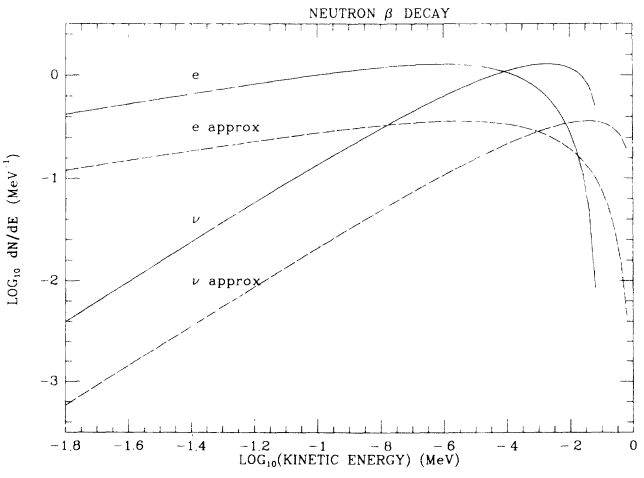

FIG. 6. The electron and electron-neutrino spectra produced in neutron β-decay spectra. The solid lines use $\Delta=1.293$ MeV and $m_e=0.511$ MeV. The dashed lines are for the approximation used in the jet code, $\Delta=2$ MeV and $m_e=1$ MeV.

TABLE VI. The approximate number of final collider states produced by an initial $q\bar{q}$ pair with a center-of-mass energy of $2Q=29$ GeV. The π^0 states also include the η decays.

π^0 6.06	π^+ 5.29	π^- 5.29	p 0.25
(η 0.78)	n 0.22	$\bar{p}$ 0.25	$\bar{n}$ 0.21
K^+ 0.64	K^- 0.64	K_S^0 0.61	K_L^0 0.61

stants A and $\Lambda_{\rm QH}$ must be experimentally determined. Then, for $Q \gtrsim Q_c^2/2\mu$, $dg_{jh}(Q,E)/dE$ peaks at

$$E_{\rm peak} \sim (\mu Q/2) e^{-A(\ln Q/\Lambda_{\rm QH})^{3/2}}, \qquad y_{\rm peak} = y_0 - \sigma^2 . \tag{23}$$

An increase in the initial quark or gluon energy Q is now damped at $E_{\rm peak}$ by the exponential term in Eq. (23). For pions—the major contributors to the final electron, photon, and neutrino spectra for at least $Q \leq 100$ GeV—and protons, the exponential term ensures that $E_{\rm peak}$ remains of the order of m_h. $E_{\rm peak}$ is almost stationary as a function of Q for $\pi^\pm$ and increases slightly for $p\bar{p}$.

When the hadrons are relativistic, the behavior of dg_{jh}/dE above $E_{\rm peak}$ can be described via a Drell-Yan-West relation[34]

$$\frac{dg_{jh}}{dE} \propto \frac{1}{E}\left[1-\frac{E}{Q}\right]^{2m-1} . \tag{24}$$

(Again for nonrelativistic hadrons, E should be replaced by the momentum.) Here m is the number of "spectator quarks" q_s required for the e^+e^- annihilation event $e^+e^-(+q_s)\to q\bar{q}(+q_s)\to h+X$, i.e., $m=1$ for mesons ($q\bar{q}_s$ or $\bar{q}q_s$) and $m=2$ for baryons (qq_sq_s or $\bar{q}\bar{q}_s\bar{q}_s$). For

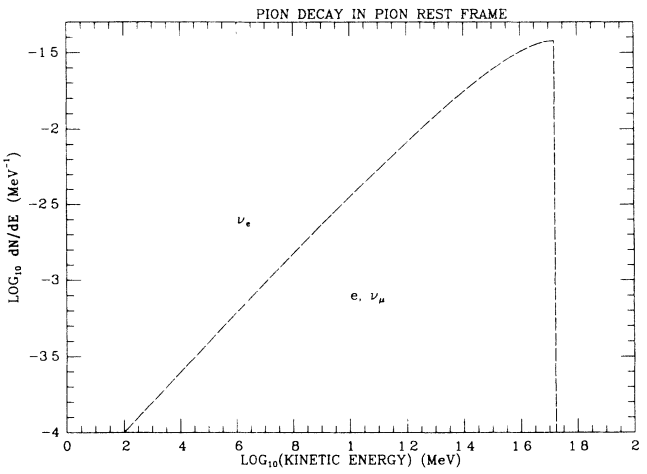

FIG. 7. The electron, muon- and electron-neutrino $\pi^\pm$ decay spectra in the pion rest frame.

$0.4 \leq E/Q \leq 0.8$ the experimental data suggest[35] that $1 \leq 2m-1 \leq 2$ when averaged over all $q\bar{q}$ jet events.

Combining the above, a reasonable approximation to the fragmentation function for general Q is

$$\frac{dg_{jh}}{dE} = \frac{G}{E}\left[1-\frac{E}{Q}\right]^{2m-1} \Theta(E-km_hc^2) , \tag{25}$$

where Θ is the Heaviside function, $km_hc^2 = O(m_hc^2)$ is the position of the peak and G is a normalizing constant which depends on the initial and final species. [Strictly speaking, Eq. (25) is only valid in the relativistic limit.]

TABLE VII. The peaks of $T=0.3$–100 GeV flux plotted in Fig. 4.

T (GeV)		$p\bar{p}$	$e^\pm$	γ	$\nu\bar{\nu}$
0.3	Peak flux ($\rm GeV^{-1}$ $\rm sec^{-1}$)	7.3(±0.4) $\times 10^{22}$	1.43(±0.07) $\times 10^{24}$	9.1(±0.5) $\times 10^{23}$	4.6(±0.2) $\times 10^{24}$
	at $E_{\rm peak}$ (GeV)	0.076 (±0.009)	0.030 (±0.003)	0.067 (±0.004)	0.028 (±0.002)
1	Peak flux ($\rm GeV^{-1}$ $\rm sec^{-1}$)	3.0(±0.2) $\times 10^{23}$	1.14(±0.06) $\times 10^{25}$	7.1(±0.4) $\times 10^{24}$	3.6(±0.2) $\times 10^{25}$
	at $E_{\rm peak}$ (GeV)	0.106 (±0.007)	0.028 (±0.002)	0.076 (±0.004)	0.032 (±0.002)
10	Peak flux ($\rm GeV^{-1}$ $\rm sec^{-1}$)	2.6(±0.1) $\times 10^{24}$		1.37(±0.10) $\times 10^{26}$	7.1(±0.5) $\times 10^{26}$
	at $E_{\rm peak}$ (GeV)	0.35 (±0.05)		0.062 (±0.004)	0.027 (±0.002)
50	Peak flux ($\rm GeV^{-1}$ $\rm sec^{-1}$)	1.8(±0.1) $\times 10^{25}$		1.1(±0.05) $\times 10^{27}$	6.0(±0.3) $\times 10^{27}$
	at $E_{\rm peak}$ (GeV)	0.46 (±0.03)		0.068 (±0.005)	0.022 (±0.002)
100	Peak flux ($\rm GeV^{-1}$ $\rm sec^{-1}$)	4.3(±0.2) $\times 10^{25}$		2.4(±0.1) $\times 10^{27}$	1.38(±0.05) $\times 10^{28}$
	at $E_{\rm peak}$ (GeV)	0.46 (±0.06)		0.075 (±0.015)	0.020 (±0.002)

Substituting Eq. (25) into the instantaneous emission integral, Eq. (16), and noting that $\Gamma_s \propto Q^2T^{-2}$ in the relativistic regime, the flux of h hadrons produced by the decay of the evaporated quarks or gluons is then approximately

$$\frac{d\dot{N}_h}{dE} \propto \int_E^\infty \frac{Q^2T^{-2}E^{-1}(1-E/Q)^{2m-1}\Theta(E-km_hc^2)}{\exp(Q/T)\pm 1}dQ . \tag{26}$$

Thus we would expect the following.

(i) For $E \simeq km_hc^2 \ll T$, the major contribution comes from $Q \simeq km_hc^2$ where $\exp(Q/T) \simeq 1$. The shape of the curve will be determined by the form of the fragmentation peak for low Q.

(ii) For $km_hc^2 \ll E \sim T$, $(Q/T)^2/[\exp(Q/T)\pm 1]$ peaks at $Q/T \simeq 1.5$–2 and so $Q \simeq T$ produces the major effect, giving $d\dot{N}_h/dE \propto E^{-1}$.

(iii) For $T \ll E$, if we approximate $[\exp(Q/T)\pm 1]^{-1}$ by $e^{-Q/T}$ and note that the lower bound of the integral dominates, we have $d\dot{N}_h/dE \propto E^2e^{-(E/T)}$.

If the primary emitted particle is a nondecaying species, then we replace dg_{jh}/dE by $\delta(E-Q)$ and so (i) for $E \ll T$, assuming $\Gamma_s \propto E^2T^{-2}$ for $s=\frac{1}{2}$ and $s=0$, we have $d\dot{N}/dE \propto E$ if $s=0$ and $d\dot{N}/dE \propto E^2$ if $s=\frac{1}{2}$. These are only approximate, since Γ_s falls off more steeply than $E^2\sigma_g$ as $E/T \to 0$, the slope is slightly steeper at lower energies. Also, since $\Gamma_{s=1} \propto E^4T^{-4}$ as $E/T \to 0$, $d\dot{N}_d/dE \propto E^3$ for $s=1$.

(ii) For $E \gg T$ and all s, $d\dot{N}_d/dE \propto E^2e^{-(E/T)}$.

IV. NUMERICAL SIMULATION OF JET EMISSION AND FRAGMENTATION

A. Simulation of emission

To simulate the final emission spectra, we convolve the Hawking emission formula with a Monte Carlo jet code, based on Refs. 33 and 34, which was written to describe accelerator e^+e^- annihilation events. Our program creates n fundamentally evaporated particles and their decays. (Here n is the unweighted number of evaporated particles.) We randomly generate with equal probability a $\nu\bar{\nu}$, γ, $e^\pm$, $\mu^\pm$, $\tau^\pm$, gluon or quark flavor or, if pions are directly emitted, a $\pi^\pm$ or π^0. The particle is then weighted by its degrees of freedom and the relative integrated flux of $s=0$, $\frac{1}{2}$, or 1 particles per helicity state. We make no distinction between the three neutrino species.

The energy of the particle Q is found using a standard Monte Carlo technique. A value for $X=Q/T$ is first randomly chosen between 0 and $X_{\max}$, the maximum value of Q/T in the program, and then constrained to have the Hawking distribution

$$H(X)=\frac{\sigma_s(X)X^2}{\exp(X)-(-1)^{2s}} . \tag{27}$$

We accomplish this by requiring that $H(X) \geq H_{\max}R$ where R is a random number between 0 and 1 and $H_{\max} \geq$ the maximum of $H(X)$ for all X. We use the absorption cross sections, σ_s, calculated by Page[24] and Simpkins[26] for $s=0$, $\frac{1}{2}$, and 1. The QCD jet code, BIGWIG, then decays the particle. Actually, we initially create a particle-antiparticle jet with a center-of-mass en-

TABLE VIII. The peaks of the $T=0.3$–100 GeV power plotted in Fig. 5.

T (GeV)		$p\bar{p}$	$e^\pm$	γ	$\nu\bar{\nu}$
0.3	Peak power ($\sec^{-1}$)	9.1(±0.5) $\times 10^{21}$	8.6(±0.4) $\times 10^{22}$	1.02(±0.05) $\times 10^{23}$	2.48(±0.12) $\times 10^{23}$
	at E'_{peak} (GeV)	0.200 (±0.015)	0.106 (±0.006)	0.188 (±0.012)	0.090 (±0.010)
1	Peak power ($\sec^{-1}$)	7.5(±0.4) $\times 10^{22}$	7.4(±0.4) $\times 10^{23}$	8.5(±0.4) $\times 10^{23}$	2.1(±0.1) $\times 10^{24}$
	at E'_{peak} (GeV)	0.45 (±0.02)	0.119 (±0.007)	0.224 (±0.007)	0.112 (±0.006)
10	Peak power ($\sec^{-1}$)	2.35(±0.12) $\times 10^{24}$	1.86(±0.13) $\times 10^{25}$	2.37(±0.17) $\times 10^{25}$	5.5(±0.4) $\times 10^{25}$
	at E'_{peak} (GeV)	2.14 (±0.05)	0.245 (±0.015)	0.43 (±0.04)	0.214 (±0.015)
50	Peak power ($\sec^{-1}$)	2.6(±0.1) $\times 10^{25}$	1.84(±0.09) $\times 10^{26}$	2.3(±0.1) $\times 10^{26}$	5.5(±0.3) $\times 10^{26}$
	at E'_{peak} (GeV)	3.5 (±0.5)	0.40 (±0.03)	0.77 (±0.06)	0.34 (±0.03)
100	Peak power ($\sec^{-1}$)	6.6(±0.3) $\times 10^{25}$	4.6(±0.2) $\times 10^{26}$	5.7(±0.3) $\times 10^{26}$	1.35(±0.07) $\times 10^{27}$
	at E'_{peak} (GeV)	7.9 (±1.5)	0.56 (±0.05)	0.89 (±0.06)	0.44 (±0.05)

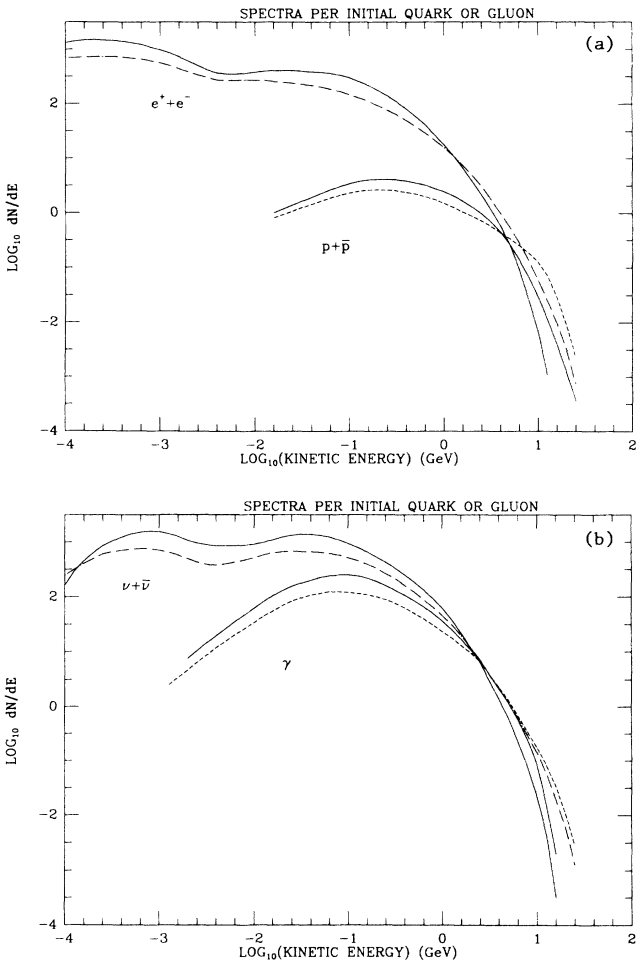

FIG. 8. The final distributions produced by jets with initial energy $Q=40$ GeV. The solid curves represent the states produced per initial gluon jet. The dashed curves represent the states produced per initial quark jet, averaged over five flavors.

ergy of $E_{\text{c.m.}}=2Q$. This is to balance the color and electric charge in the final clustering phases in the decay process. At all previous stages in the decay process, however, the particle and antiparticle jets can be regarded as independent. We modified BIGWIG to decay the jet products down to the species which are stable on astrophysical time scales, ($p\bar{p}$, $e^{\pm}$, γ, and $\nu\bar{\nu}$), and to decay the primary emitted $\mu^{\pm}$, $\tau^{\pm}$, $\pi^{\pm}$, and π^0. Our version also saves time and computer space in the decay phase by storing only the latest decay products at each fragmentation stage. If, after a few hundred attempts to find a decay mode, BIGWIG is still unfruitful, we return to the start of the program and generate a new initial particle. This only happens when Q is very close to the rest mass of the initial particle. Typically, our programs take $n \simeq 35{,}000$–$45{,}000$ and $X_{\max}=8.5$–10.

B. Simulation of jet fragmentation

The BIGWIG code[33,34] was developed for high-energy (GeV) e^+e^- annihilation. In the collider, e^+ and e^- annihilate to produce quark and antiquark and, occasionally, gluon jets which then decay into the observed hadrons. BIGWIG is based on a perturbative QCD parton branching mechanism with an accurate treatment of leading collinear and infrared singularities and conserves center-of-mass energy. After creating a jetlike cascade of partons nearer to on-shell mass, hadronization occurs via the preconfinement and decay of color-singlet clusters. The program generates two jet, particle-antiparticle configurations together with a leading-log approximation to multijets. Although tightly constrained, it gives a good account of the existing data for center-of-mass energies 3.6–40 GeV. (A collider center-of-mass energy of 3.6 GeV corresponds to initial quark energies of 1.8 GeV or the peak energy from a $T \simeq 0.4$ GeV hole.) BIGWIG neglects the finite width of resonances (short-lived particles states) and uses instead central masses. The treatment of resonance decays also omits the spin-polarized terms which are relevant when particles have angular momentum. The perturbative parton branching approach may have a 30% inaccuracy where the matrix elements are small, e.g., in the high-momentum tails of the distributions. The QCD running coupling constant is approximated by $\alpha_s = 12\pi/[(33-2n_j)\ln(4Q^2/\Lambda^2_{\text{QH}})]$ where n_j is the maximum number of flavors (i.e., 5 or 6) and $2Q$ is BIGWIG's initial center-of-mass energy (instead of the parton center-of-mass energy at each branching). The weak, e.g., neutron beta, decays assume pointlike $V-A$ matrix elements.

Our $T<10$ GeV programs use the five-flavor version of BIGWIG described in Ref. 33. The $T \geq 10$ GeV runs use a

TABLE IX. The errors in plotting $d\dot{N}/dE$ and $E\,d\dot{N}/dE$ as a function of E (in GeV) for the $Q=40$ GeV quark and gluon jets of Fig. 8. The errors at all other energies are less than 10%.

$T=0.1$ GeV		$p\bar{p}$	$e^{\pm}$	γ	$\nu\bar{\nu}$
Flux	Quark	30% for $E<0.06$	20% for $E>6$	20% for $E>5$	30% for $E>10$
	Jet	20% for $E>6$			
	Gluon	30% for $E<0.1$	20% for $E<0.01$	20% for $E>3$	30% for $E>1$
	Jet	20% for $E>5$	20% for $E>5$		
Power	Quark	30% for $E<0.1$	30% for $E>2$	20% for $E<0.01$	20% for $E<0.001$
	Jet	20% for $E>10$		20% for $E>10$	20% for $E>10$
	Gluon	40% for $E<0.25$	20% for $E<0.003$	20% for $E<0.01$	20% for $E<0.001$
	Jet	30% for $E>3$	20% for $E>5$	20% for $E>5$	20% for $E>2$

TABLE X. Distributions of flux and power, multiplicities and average kinetic energies in $Q=40$ GeV quark and gluon jets.

$Q=40$ GeV		$p\bar{p}$	$e^{\pm}$	γ	$\nu\bar{\nu}$
Flux	Quark	1.47%	19.72%	21.86%	56.96%
	Jet	(±0.01%)	(±0.07%)	(±0.08%)	(±0.16%)
	Gluon	1.55%	19.54%	22.15%	56.76%
	Jet	(±0.03%)	(±0.13%)	(±0.14%)	(±0.29%)
Power	Quark	9.19%	16.61%	29.94%	44.26%
	Jet	(±0.20%)	(±0.21%)	(±0.33%)	(±0.72%)
	Gluon	9.18%	15.89%	32.43%	42.50%
	Jet	(±0.31%)	(±0.29%)	(±0.61%)	(±0.94%)
Multiplicities	Quark	0.755	10.16	11.22	29.25
	Jet	(±0.007)	(±0.03)	(±0.04)	(±0.08)
	Gluon	1.22	15.47	17.45	44.71
	Jet	(±0.02)	(±0.07)	(±0.11)	(±0.21)
$\bar{E}$ (GeV)	Quark	3.94	0.655	1.067	0.605
	Jet	(±0.03)	(±0.002)	(±0.002)	(±0.005)
	Gluon	2.08	0.412	0.744	0.380
	Jet	(±0.03)	(±0.001)	(±0.003)	(±0.003)

more sophisticated, generalized version,[36] HERWIG, which includes the predicted but still unobserved top quark. (HERWIG also includes options for hard lepton-lepton, lepton-hadron, and hadron-hadron scattering and soft hadron-hadron collisions which are irrelevant here.) The charged multiplicity produced by HERWIG using 10^4 events matches the analytic QCD predictions to within the statistical errors up to 10 TeV. The results agree similarly with the experimental data at the presently accessible energies (up to center-of-mass energies of $2Q \simeq 46$ GeV). Comparisons with the Mark II (Ref. 37) data at $2Q=29$ GeV show that the charged-particle momentum (p) distributions match the experimental data, to within the statistical errors, at all but very high $x=p/Q$. The discrepancy is only significant when $x \gtrsim 0.7$. The distributions as $x \rightarrow 1$ may be underestimated by a factor of 3. The discrepancy arises only in HERWIG and not in BIGWIG and may be corrected for in further versions by varying the effective quark masses at these energies. [This discrepancy, though, should have little effect on the final emission spectra: this is, first, because the distribution falls off steeply away from the low x maximum (for example, the true dN/dE at $x=0.8$ is about 6 orders of magnitude below dN/dE at $x \rightarrow 0$); and second, the jet spectra must be convolved with the Hawking distribution.] For both BIGWIG and HERWIG the low-Q matching is more uncertain since the experimental data are scarce. This is also true for $p\bar{p}$. We should stress that the quality of the matching depends on the choice of parameters for the effective quark and gluon masses, $\Lambda_{\rm QH}$ and the cluster mass parameter (minimum off-shellness) at which the perturbative branching is halted. To achieve the best match, BIGWIG uses $m_{u,d}=0.300$ GeV, $m_s=0.500$ GeV, $m_g=0.600$ GeV, $m_c=1.87$ GeV, and $m_b=5.20$ GeV. HERWIG uses $m_{u,d}=0.320$ GeV, $m_s=0.500$ GeV, $M_g=0.650$ GeV, $m_c=1.80$ GeV, $m_b=5.20$ GeV, and $m_t=50.0$ GeV.

In summary, we take 10% as an upper estimate of any systematic error in the dN/dE spectra produced by the programs, except at high x since this is the estimated statistical error in the distributions below $x \lesssim 0.5$ for 10^4 events quoted in Ref. 36. At high x, the statistical errors in our programs will be comparable with any systematic error since so few high-x particles are generated and the statistical error at a given E is proportional to the square root of the entries in the histogram bin. Any systematic error is $\ll 10\%$ around the peaks[36] in the distributions.

C. Normalization and error estimates of results

Since our program generates more than one quasirandom statistical distribution, we desire an independent,

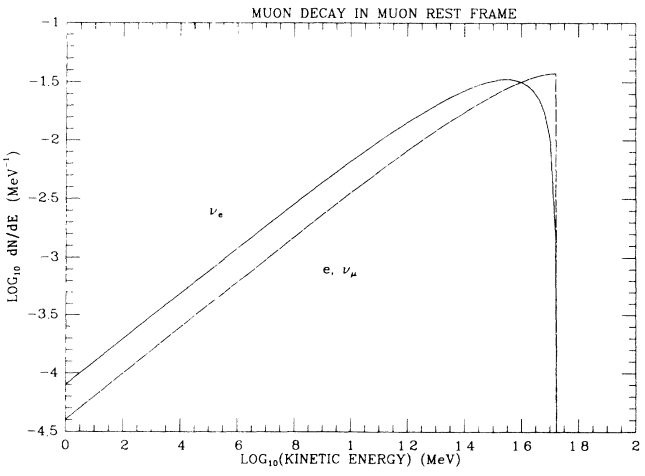

FIG. 9. The e, $\bar{\nu}_e$, and $\bar{\nu}_\mu$ muon decay spectra in the muon rest frame.

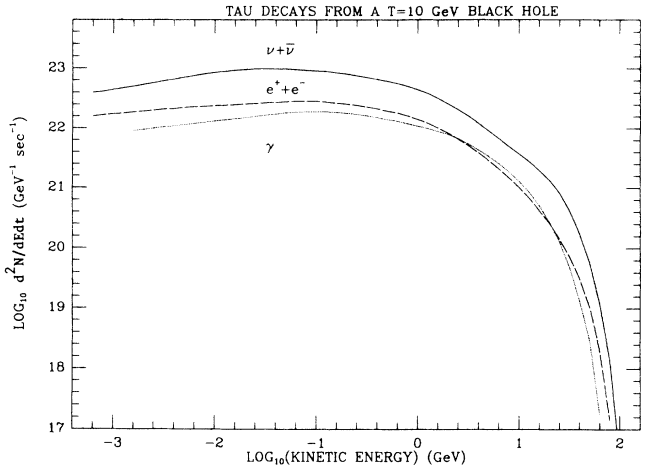

FIG. 10. The decays of the $\tau^{\pm}$ emission from a $T=10$ GeV black hole.

nonstatistical method to normalize the black-hole emission. This will help to minimize the total statistical error although the shape of the spectra and the relative number in each species will still contain statistical fluctuations. To do this, we normalize the combined primary and decay emission by matching the peak in the directly emitted $s=\frac{1}{2}$ flux to the value calculated by Page for relativistic electrons [see Eq. (8)]. The power spectra can also be independently normalized by matching the peak in the direct $s=\frac{1}{2}$ power to Page's value given in Eq. (9). The difference between the two normalizing factors is an estimate of the error in the normalization. For our $T=0.02-100$ GeV programs with $n=35{,}00-45{,}000$ events, the error is between (0.4–6.5)%. Thus we choose to normalize the flux and power spectra with the average of the two factors. Our method is also checked by matching the number of directly emitted neutrinos to Page's value to obtain another normalization factor. For $T=0.02-100$ GeV with $n=35{,}000-45{,}000$, the variation is between (0.2–6.3)%, less than the calculated statistical errors in the normalizing factors.

Using the means and the histograms of the spectra, we can calculate the relative numbers and energies of the final states and the fractions of these which are jet products. If $P(y)$ is the mean of a weighted distribution y, the error associated with P is RMS$=\sqrt{P\{[y-P(y)]^2\}}$ divided by the square root of the total unweighted number of histogram entries. To calculate[38] the error in the integrated flux (and power) for each species, let N be the number of times the program produces a given final species and let w be the spin- and temperature-dependent weight for each event. The quantity we use to obtain the flux (or power) is then $W=\sum_{\text{all events}} w=N\bar{w}$ where $\bar{w}$ is the (unweighted) mean of w. An estimate of the error in W is $\delta W=\sqrt{N^2(\delta\bar{w})^2+\bar{w}^2(\delta N)^2}$ where $\delta\bar{w}=(\overline{w^2}-\bar{w}^2)^{1/2}/\sqrt{N}$ is an estimate of the error in $\bar{w}$ and $\delta N\simeq\sqrt{N}$ is an estimate of the error in N. If $w_{\max}$ is the maximum value of w, this gives

$$\delta W\leq\sqrt{N}\,w_{\max}\ . \tag{28}$$

Since our programs store W, N, and $\bar{w}$ but not $\delta\bar{w}$, we use (28) as the estimate for δW although in general it is an overestimate. For the instantaneous spectra, we have $0.6\lesssim w\lesssim 12$ and so (28) overestimates δW by, at most, a factor of about 2. Equation (28) is also an upper estimate for the statistical error in the entries per histogram bin if N is replaced by the number of unweighted entries in the bin.

V. RESULTS OF NUMERICAL SIMULATION

A. The $T=0.3-100$ GeV emission

The $p\bar{p}$, $e^{\pm}$, γ, and $\nu\bar{\nu}$ flux from $T=0.3$, 1, 10, 50, and 100 GeV black holes is presented in Fig. 4. (These temperatures correspond to $M=3.53\times10^{13}$ g, 1.06×10^{13} g, 1.06×10^{12} g, 2.12×10^{11} g, and 1.06×10^{11}g, respectively.) We plot $\log d\dot{N}/dE$ vs $\log E$ where E is the total energy for γ and $\nu\bar{\nu}$, and the kinetic energy for $p\bar{p}$ and $e^{\pm}$. The power spectra, $\log E d\dot{N}/dE$ vs $\log E$, are shown in Fig. 5. All spectra combine particles and antiparticles. They include the final decay states as well as the directly emitted $e^{\pm}$, γ, or $\nu\bar{\nu}$. We have assumed that quarks, gluons, photons, and three lepton families can be directly emitted provided Q is greater than the relevant rest masses: for example, a $T=0.3$ GeV hole emits $e^{\pm}$, γ, $\nu_{e,\mu,\tau}$, $\mu^{\pm}$, q_u, q_d, q_s, q_c, g,and $\tau^{\pm}$ in significant numbers, since the direct energy peaks at $E_{\text{peak}}\simeq1.21$ GeV for $s=\frac{1}{2}$ and $E_{\text{peak}}\simeq1.74$ GeV for $s=1$. For $T=1$ GeV, the list in-

TABLE XI. The errors in plotting $d\dot{N}/dE$ and $E\,d\dot{N}/dE$ with E in GeV for $T=0.1$ GeV. Case (i) includes primary pions; case (ii) does not. The errors at all other energies are less than 10%.

$T=0.1$ GeV		$p\bar{p}$	$e^{\pm}$	γ	$\nu\bar{\nu}$
(i)	Flux	60% all E	25% for $E<0.01$ 10% for $E>0.6$	10% for $E<0.02$ 10% for $E>0.6$	10% for $E<0.01$ 20% for $E>0.6$
	Power	60% all E	30% for $E<0.005$ 20% for $E>0.6$	10% for $E<0.016$ 20% for $E>0.6$	20% for $E<0.005$ 20% for $E>0.6$
(ii)	Flux	60% all E	25% for $E<0.01$ 10% for $E>0.6$	10% for $E<0.02$ 10% for $E>0.6$	10% for $E<0.01$ 20% for $E>0.6$
	Power	60% all E	30% for $E<0.005$ 20% for $E>0.6$	20% for $E<0.016$ 20% for $E>0.6$	20% for $E<0.005$ 20% for $E>6$ GeV

cludes q_b, and at higher T, q_b and q_t. The $T=50-100$ GeV black holes also emit $W^{\pm}$ and Z^0 bosons, which we have omitted here. This has a negligible effect on the spectra since there are far fewer $W^{\pm}$ and Z^0 degrees of freedom than quark and gluon degrees of freedom. We discuss the q_t and weak-boson emission, as well as hypothetical particles, in Sec. V D.

1. General overview

The dominant features of the spectra are as follows.

(a) The low-energy peaks in the lepton spectra which come from neutron β decay in the jets.

(b) The 0.01–10 GeV lepton and photon peaks which predominantly come from the jet π^+, π^-, and π^0 decays.

(c) The relatively insignificant direct $e^{\pm}$, γ, and $\nu\bar{\nu}$ emission at $E \simeq 5T$.

The spectra differ markedly from the calculations of previous authors in having the significant low and middle energy contributions (a) and (b). The jet pions decays dominate the total flux. The smaller $\bar{p}p$ spectra do not resemble the other spectra since the protons are not emitted directly nor produced in pion decays. The $p\bar{p}$ flux has a slope of about $E^{0.5}$ at low energies, an E^{-1} slope at 0.3 GeV $\lesssim E \lesssim T$ and the exponential cutoff of the Hawking distribution at high energies. The $p\bar{p}$ power correspondingly has an $E^{1.5}$ slope at low energies. At all but the highest energies, where the exponential tail of the Hawking distribution is manifest, all spectra reflect the relevant decay spectra. Since they involve the superposition of more than one decay, we cannot easily make out distinct slopes. The γ power, however, has an $E^{1.5}$ slope for $0.003 \lesssim E \lesssim 0.3$ GeV, coming from the jet π^0 distributions, and the γ flux appears to have the corresponding $E^{0.5}$ to E^1 slope for $E \lesssim 0.01$ GeV. The $e^{\pm}$, γ, and $\nu\bar{\nu}$ fluxes have slopes of about E^{-1} between $0.1 \lesssim E \lesssim T$ GeV, also arising from the jet fragmentation distributions.

The possible errors in the plots are summarized in Table I. These errors represent the accuracy with which a line can be fitted to a histogram and are determined purely by inspection. They are a generous estimate of the statistical error in the plots. At all energies other than those referred to in the table, the error is less than 10%. In general, at low energies, the statistical error in the flux is greater than the error in the power since the flux is constructed from the power by dividing by E. *All errors quoted in any context in Sec. V are statistical errors.* To them must be added the 10% upper estimate of possible systematic errors in the jet code (except on the tails of the distributions where the statistical errors anyway swamp any systematic errors). Also, the spectra should not be relied on below 1 MeV since BIGWIG only stores particle

TABLE XII. Distributions of total flux and power, multiplicities and average kinetic energies for $T=0.1$ GeV: case (i) with primary pion emission.

$T=0.1$ GeV	$p\bar{p}$	$e^{\pm}$	γ	$\nu\bar{\nu}$
Flux (% of $\dot{N}_{\rm tot}$)	0.02% (±0.005%)	23.03% (±0.47%)	18.31% (±0.41%)	58.64% (±0.91%)
		$\dot{N}_{\rm tot}=9.62(\pm0.17)\times10^{22}$ GeV^{-1} sec^{-1}		
Jet products (% of $\dot{N}_{\rm tot}$)	0.02% (±0.005%)	12.82% (±0.67%)	15.35% (±0.53%)	38.04% (±1.23%)
Power (% of $P_{\rm tot}$)	0.17% (±0.05%)	25.69% (±0.87%)	22.65% (±0.81%)	51.49% (±1.58%)
		$\dot{P}_{\rm tot}=1.42(\pm0.04)\times10^{22}$ sec^{-1}		
Jet products (% of $P_{\rm tot}$)	0.17% (±0.05%)	9.29% (±1.38%)	18.62% (±1.02%)	25.47% (±2.33%)
Peak flux (GeV^{-1} sec^{-1})	$3(\pm2)\times10^{20}$	$1.35(\pm0.07)\times10^{23}$	$8.1(\pm0.4)\times10^{22}$	$4.3(\pm0.2)\times10^{23}$
at $E_{\rm peak}$ (GeV)	0.04 (±0.02)	0.032 (±0.002)	0.072 (±0.003)	0.032 (±0.007)
Peak power (sec^{-1})	$2(\pm1)\times10^{19}$	$8.0(\pm0.4)\times10^{21}$	$8.2(\pm0.4)\times10^{21}$	$2.2(\pm0.1)\times10^{22}$
at $E'_{\rm peak}$ (GeV)	0.076 (±0.015)	0.095 (±0.012)	0.170 (±0.008)	0.083 (±0.004)
Multiplicities	0.001 (±0.001)	0.735 (±0.010)	0.585 (±0.010)	1.867 (±0.007)
$\bar{E}$ (GeV)	0.109 (±0.004)	0.164 (±0.001)	0.183 (±0.001)	0.130 (±0.001)

rest masses to 1 MeV. We note that, since the spectra are plotted on log-log axes, errors of less than a factor of 2 cannot significantly change the shape of the spectra.

Tables II and III display the $p\bar{p}$, $e^{\pm}$, γ, and $\nu\bar{\nu}$ flux and power at each temperature. For $T=0.3-100$ GeV, the final states are emitted in ratios of about 2.1($\pm$0.3%) $p\bar{p}$, 19.9($\pm$0.7%) $e^{\pm}$, 21.5($\pm$1%) γ, and 56.5($\pm$0.8%) $\nu\bar{\nu}$. Since the evaporation process and the decays conserve CP at these temperatures, equal numbers of particles and antiparticles are produced. The total flux of final states increases by more than 3 orders of magnitude between $T=0.3$ and 100 GeV. At $T=1$ GeV, 95.1($\pm$0.6%) of the particles are jet products; at $T=50$ GeV, 99.4($\pm$0.4%) are jet products. The power is carried in ratios of about 10.5($\pm$1.7%) $p\bar{p}$, 19.5($\pm$1.2%) $e^{\pm}$, 24.3($\pm$1.2%) γ, and 45.7($\pm$1.2%) $\nu\bar{\nu}$. The fluctuations in the ratios with temperature reflect the different jet decay dynamics in each regime but there is no overall trend. The total power increases by 5 orders of magnitude from $T=0.3$ GeV to $T=100$ GeV. The nonjet power is (19–26) % of the total. This agrees well with Eqs. (10) and (11) although BIGWIG introduces each new quark flavor gradually as T approaches the effective rest mass. The nonjet contribution to the power is still sizable since the directly emitted energy peaks at $E\simeq 5T$, well above the average energy of the decay products.

The average number of final particles per fundamentally emitted particle (which we define here to be the multiplicity) increases substantially between $T=0.3$ and 100 GeV (see Table IV). This is most notable for the neutrinos. Roughly $24e^{\pm}$, 27γ, and $68\nu\bar{\nu}$ are produced per emitted particle at $T=100$ GeV. The average $p\bar{p}$ multiplicity increases from about 0.1 at $T=0.3$ GeV to 2.9 at $T=100$ GeV. Almost all particles in each species are jet products: if only $e^{\pm}$, γ, $\nu_{e,\mu,\tau}$, $\mu^{\pm}$, and $\tau^{\pm}$ were directly emitted, the average multiplicities would be $0p\bar{p}$, $0.70e^{\pm}$, 0.37γ, and $1.70\nu\bar{\nu}$. Renormalizing to include five quark flavors and the gluons, the nonjet contribution to the above multiplicities is $0p\bar{p}$, $0.17e^{\pm}$, 0.07γ, and $0.41\nu\bar{\nu}$, or for six quark flavors, $0p\bar{p}$, $0.15e^{\pm}$, 0.06γ, and $0.36\nu\bar{\nu}$. As the multiplicities per emitted particle increase with temperature, the number of fundamentally emitted particles also increases—on the one hand, because more particle species are emitted at higher T and, on the other, because for each helicity state $\int d\dot{N}/dE\,dE \propto T$. Together, these increase the total flux by more than 3 orders of magnitude between $T=0.3$ and 100 GeV.

We can parametrize the total flux for $T=0.3-100$ GeV by

$$\dot{N}_{\rm tot}\simeq 1.0(\pm 0.3)\times 10^{25}\left[\frac{T}{\rm GeV}\right]^{1.6\pm 0.1}\ {\rm sec}^{-1} \qquad (29)$$

with

TABLE XIII. Distributions of total flux and power, multiplicities and average kinetic energies for $T=0.1$ GeV: case (ii) without primary pion emission.

$T=0.1$ GeV	$p\bar{p}$	$e^{\pm}$	γ	$\nu\bar{\nu}$
Flux	0.01% ($\pm$0.004%)	23.37% ($\pm$0.45%)	18.18% ($\pm$0.38%)	58.43% ($\pm$0.86%)
		$\dot{N}_{\rm tot}=8.30(\pm 0.13)\times 10^{22}$ GeV^{-1} sec^{-1}		
Jet products (% of $\dot{N}_{\rm tot}$)	0.01% ($\pm$0.004%)	14.35% ($\pm$0.63%)	17.51% ($\pm$0.45%)	42.67% ($\pm$1.12%)
Power	0.07% ($\pm$0.03%)	25.79% ($\pm$0.83%)	22.17% ($\pm$0.73%)	51.98% ($\pm$1.49%)
		$P_{\rm tot}=1.31(\pm 0.03)\times 10^{22}$ sec^{-1}		
Jet products (% of $P_{\rm tot}$)	0.07% ($\pm$0.03%)	9.60% ($\pm$1.32%)	19.76% ($\pm$1.03%)	26.01% ($\pm$2.20%)
Peak flux (GeV^{-1} sec^{-1})	$6(\pm 4)\times 10^{20}$	$1.07(\pm 0.07)\times 10^{23}$	$6.0(\pm 0.4)\times 10^{22}$	$3.2(\pm 0.2)\times 10^{23}$
at $E_{\rm peak}$ (GeV)	0.02 ($\pm$0.015)	0.028 ($\pm$0.003)	0.072 ($\pm$0.006)	0.032 ($\pm$0.004)
Peak power (sec^{-1})	$1.7(\pm 1)\times 10^{19}$	$7.0(\pm 0.5)\times 10^{21}$	$7.3(\pm 0.5)\times 10^{21}$	$1.9(\pm 0.1)\times 10^{22}$
at $E'_{\rm peak}$ (GeV)	0.038 ($\pm$0.020)	0.140 ($\pm$0.015)	0.23 ($\pm$0.02)	0.126 ($\pm$0.011)
Multiplicities	0.001 ($\pm$0.001)	0.73 ($\pm$0.01)	0.57 ($\pm$0.01)	1.828 ($\pm$0.006)
$\bar{E}$ (GeV)	0.034 ($\pm$0.001)	0.173 ($\pm$0.001)	0.193 ($\pm$0.001)	0.141 ($\pm$0.001)

$$\dot{N}_{p\bar{p}} \simeq 2.1(\pm 0.4)\times 10^{23}\left[\frac{T}{\text{GeV}}\right]^{1.6\pm 0.1} \text{sec}^{-1} ,$$
$$\dot{N}_{e^{\pm}} \simeq 2.0(\pm 0.6)\times 10^{24}\left[\frac{T}{\text{GeV}}\right]^{1.6\pm 0.1} \text{sec}^{-1} ,$$
$$\dot{N}_{\gamma} \simeq 2.2(\pm 0.7)\times 10^{24}\left[\frac{T}{\text{GeV}}\right]^{1.6\pm 0.1} \text{sec}^{-1} , \quad (30)$$
$$\dot{N}_{\nu\bar{\nu}} \simeq 5.6(\pm 1.7)\times 10^{24}\left[\frac{T}{\text{GeV}}\right]^{1.6\pm 0.1} \text{sec}^{-1} .$$

The total emitted power can be also parametrized by

$$P_{\text{tot}} \simeq 3.0(\pm 0.3)\times 10^{24}\left[\frac{T}{\text{GeV}}\right]^{2.1\pm 0.1} \text{GeV sec}^{-1} \quad (31)$$

with

$$P_{p\bar{p}} \simeq 3.2(\pm 0.4)\times 10^{23}\left[\frac{T}{\text{GeV}}\right]^{2.1\pm 0.1} \text{GeV sec}^{-1} ,$$
$$P_{e^{\pm}} \simeq 5.9(\pm 0.6)\times 10^{23}\left[\frac{T}{\text{GeV}}\right]^{2.1\pm 0.1} \text{GeV sec}^{-1} , \quad (32)$$
$$P_{\gamma} \simeq 7.3(\pm 0.7)\times 10^{23}\left[\frac{T}{\text{GeV}}\right]^{2.1\pm 0.1} \text{GeV sec}^{-1} ,$$
$$P_{\nu\bar{\nu}} \simeq 1.4(\pm 0.1)\times 10^{24}\left[\frac{T}{\text{GeV}}\right]^{2.1\pm 0.1} \text{GeV sec}^{-1} .$$

For comparison, the directly emitted flux and power per degree of particle freedom from Eqs. (10) are

$$\dot{N} = \begin{cases} 2.5\times 10^{22}(T/\text{GeV})\ \text{sec}^{-1}, & s=0 , \\ 9.3\times 10^{21}(T/\text{GeV})\ \text{sec}^{-1}, & s=\frac{1}{2} , \\ 2.8\times 10^{21}(T/\text{GeV})\ \text{sec}^{-1}, & s=1 , \end{cases} \quad (33)$$

$$P = \begin{cases} 7.0\times 10^{22}(T/\text{GeV})^2\ \text{GeV sec}^{-1}, & s=0 , \\ 3.9\times 10^{22}(T/\text{GeV})^2\ \text{GeV sec}^{-1}, & s=\frac{1}{2} , \\ 1.6\times 10^{22}(T/\text{GeV})^2\ \text{GeV sec}^{-1}, & s=1 . \end{cases}$$

Thus, with the huge increase in degrees of freedom and multiplicities when quarks and gluons are emitted, P_{tot} and especially $\dot{N}_{\text{tot}}$ are much more dependent on T. The true T dependence of $\dot{N}_{\text{tot}}$ and P_{tot} is probably more complicated, but we are limited here by statistical errors. We note that, for example, the charged hadron multiplicity[39,40] for a gluon jet of energy Q, in leading log QCD is proportional to $a\exp[b\sqrt{\ln(Q/\Lambda_{\text{QH}})}]+n_0$, where, from experiment,[41] $a=0.027$, $b=2.7\pm 0.28$, and $n_0=2$. Such analytic fits, however, do not easily give $\dot{N}_{\text{tot}}$ since they must be convolved with the spin-dependent Hawking distributions and the rest-mass thresholds.

The mean final energies for $T=0.3-100$ GeV (as displayed in Table V) are approximately

$$\bar{E}_{p\bar{p}} \simeq 5.2(\pm 0.5)\times 10^{-1}\left[\frac{T}{\text{GeV}}\right]^{0.8\pm 0.1} \text{GeV} ,$$
$$\bar{E}_{e^{\pm}} \simeq 2.9(\pm 0.5)\times 10^{-1}\left[\frac{T}{\text{GeV}}\right]^{0.5\pm 0.1} \text{GeV} , \quad (34)$$
$$\bar{E}_{\gamma} \simeq 3.4(\pm 0.5)\times 10^{-1}\left[\frac{T}{\text{GeV}}\right]^{0.5\pm 0.1} \text{GeV} ,$$
$$\bar{E}_{\nu\bar{\nu}} \simeq 2.4(\pm 0.5)\times 10^{-1}\left[\frac{T}{\text{GeV}}\right]^{0.5\pm 0.1} \text{GeV} .$$

The average energies of the primary emission for $n=10{,}000$ events are $\bar{E}_{s=0}=2.76(\pm 0.03)T$ GeV, $\bar{E}_{s=1/2}=4.25(\pm 0.03)T$ GeV, and $\bar{E}_{s=1}=5.70(\pm 0.03)T$ GeV where T is in GeV. Since the total emitted energy is conserved, the huge increase in the jet multiplicities as T increases implies that the average energies of the final states does not increase linearly with T: at higher T, many more particles are created per jet event and the increased jet energy is divided between a greater number of

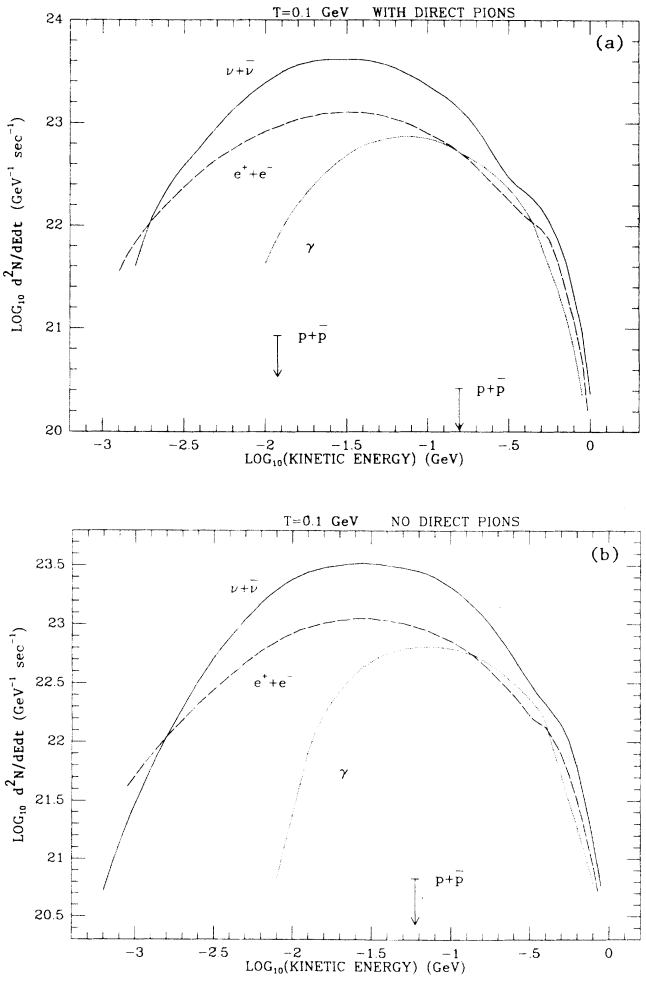

FIG. 11. The instantaneous flux and power from a $T=0.1$ GeV hole (a) with direct pion emission, (b) without direct pions. The $p\bar{p}$ point is a rough estimate, from the results, of the $p\bar{p}$ emission at that energy.

particles. As a check on our method, then, $\dot{N}_i\bar{E}_i$ is equal to P_i to well within the error estimates for $i=e^{\pm}$, γ, and $\nu\bar{\nu}$. Also $\dot{N}_{p\bar{p}}\bar{E}_{p\bar{p}}\simeq P_{p\bar{p}}$ to just within the error bounds.

2. *Neutron β-decay contribution to the spectra*

The lowest energy lepton peaks (a) come from the $n\to p+e^-+\bar{\nu}_e$, $\bar{n}\to\bar{p}+e^++\nu_e$ decays in the jets. The differential probability that a neutron produces a neutrino of total energy E_ν and momentum p_ν plus an electron of kinetic energy E_e and momentum p_e is[32] $d\Pi\propto d^3p_e d^3p_\nu\delta(E_e+m_e+E_\nu-\Delta)$ where Δ is the energy difference between the initial neutron state and the final proton state and m_e is in GeV. Thus the differential neutrino and electron number spectra are

$$\frac{dn_\nu}{dE_\nu}\propto\sqrt{(\Delta-E_\nu)^2-m_e^2}(\Delta-E_\nu)E_\nu^2\ ,$$
$$\frac{dn_e}{dE_e}\propto(E_e+m_e)\sqrt{E_e^2+2E_em_e}(\Delta-m_e-E_e)^2\ . \tag{35}$$

In the neutron's rest frame, $\Delta=m_n-\mathcal{E}_p$ where $\mathcal{E}_p$ is the total energy of the proton. The maximum momentum transfer,[42] $p=1.2$ MeV/c, implies a maximum proton kinetic energy of $E_p=p^2/2m_p\simeq10^{-6}$ GeV. Hence $\mathcal{E}_p\simeq m_p$ and $\Delta\simeq m_n-m_p=1.293$ MeV. The spectra for $\Delta=1.293$ MeV and $m_e=0.511$ MeV and also the approximations used by the jet code, $\Delta=2$ MeV and $m_e=1$ MeV, are plotted in Fig. 6. The spectra peak at $\log(E_\nu/\text{GeV})\simeq-3.2$ and $\log(E_e/\text{GeV})\simeq-3.6$, respectively. At the maxima, $dn_e/dE_e\simeq dn_\nu/dE_\nu$. The slopes below the maxima are roughly E^2 for ν and $E^{1/2}$ for $e^{\pm}$. Since the neutrons are not at rest in the jets but have a distribution of energies, the $\nu\bar{\nu}$ and $e^{\pm}$ peaks are smeared out in a frame at rest relative to the black hole.

As we remarked earlier, the slopes of the final emission at the lowest energies are those of the decay spectra. At the lowest T and E then, the $\nu\bar{\nu}$ flux should have an E^2 slope and the $e^{\pm}$ flux an $E^{1/2}$ slope. Returning to Fig. 4, we see that the $T=0.3$ and 1 GeV neutrino fluxes do indeed have a low-energy peak at $\log(E_\nu/\text{GeV})\simeq-3.2$, which we also checked is composed of ν_e and $\bar{\nu}_e$ neutrinos. Below the peaks, the $\nu\bar{\nu}$ flux and power fall off roughly as E^2 and E^3, respectively. The error created by rounding off the rest masses distorts the low-energy $e^{\pm}$ spectra but we can see that the flux peaks below $\log(E_e/\text{GeV})=-3.5$. The $e^{\pm}$ power peaks at too low an energy to determine the slopes.

Half the protons and antiprotons come from the neutron β decays. Since $m_n\simeq m_p$, most of the neutron's energy is transferred to the protons, regardless of energy, and so the neutron and proton energy distributions are almost identical. The average energy and number of neutrons and protons in a jet increases with T. This smears out the low-energy lepton flux and power peaks and increases them by 3 orders of magnitude between $T=0.3$ and 100 GeV. [The pion decay peaks (b) show a similar increase.] On the other hand, the energies at the peaks (a) change little with T. By Lorentz-transforming Eqs. (35), we can show that even for an initial neutron energy

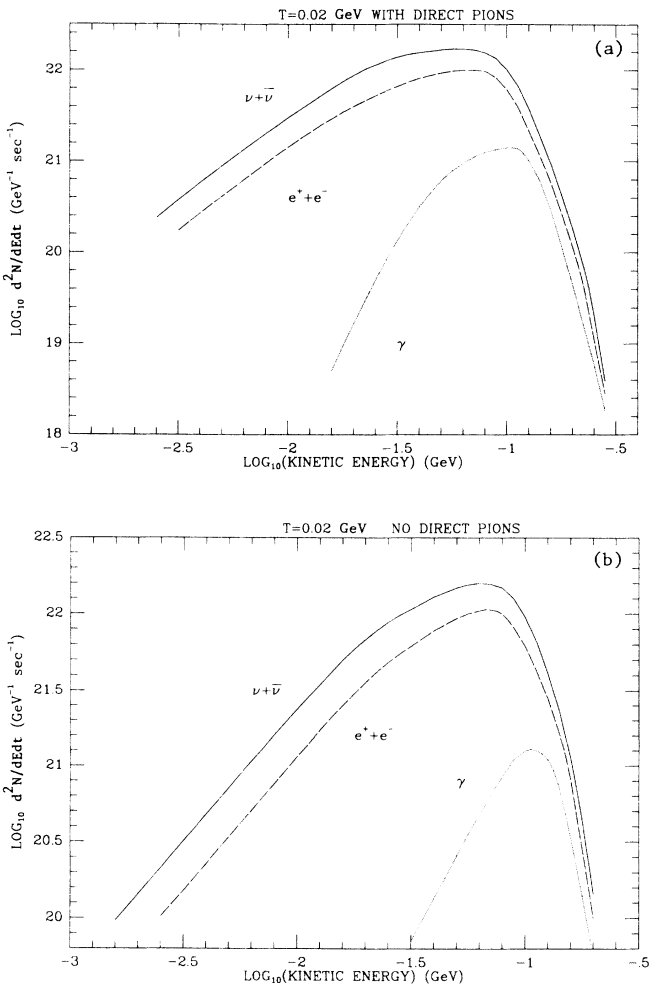

FIG. 12. The instantaneous flux and power from a $T=0.02$ GeV hole (a) with direct pion emission; (b) without direct pion emission. No $p\bar{p}$ are produced.

of 10 GeV, dn_e/dE_e peaks at about 3–10 MeV while dn_ν/dE_ν peaks below 10 MeV. However, the energy at the $p\bar{p}$ flux peak only increases by about a factor of 4 between $T=1$ and 100 GeV. Thus most of the neutrons are still nonrelativistic. The slow falloff in the $p\bar{p}$ flux at low E, especially for $T=0.3$–1 GeV, and the E^2 slope below the peaks in the $\nu\bar{\nu}$ flux also imply that most of the parent neutrons are nonrelativistic. $p\bar{p}$'s should be seen down to at least 10^{-6} GeV, the maximum kinetic energy of the proton in the neutron rest frame. Such $p\bar{p}$ are easily stopped by collisions in an accelerator. Astrophysical protons and antiprotons with energies well below the spallation threshold and long annihilation time scales, however, might be observed today if they are accelerated to much higher energies in the galactic magnetic fields,[10] for example.

3. *Jet pion decay contribution to the spectra*

The dominant 0.01–10 GeV peaks (b) come from the decay of the jet pions:

$$\pi^{\pm}\rightarrow\mu^{\pm}+\nu_{\mu}\rightarrow e^{\pm}+\nu_{e}+\nu_{\mu}+\bar{\nu}_{\mu}\ ,$$
$$\pi^{0}\rightarrow\gamma+\gamma\ . \tag{36}$$

As an example, Table VI lists the average number of baryons and mesons produced by a $q\bar{q}$ jet with a center-of-mass energy of $2Q=29$ GeV. These are the particles which are final on collider timescales. Here the numbers are averaged over five flavors where the flavors were generated in the same ratios[32] as for $e^+e^-\rightarrow q\bar{q}$. That is, $\sigma(e^+e^-\rightarrow q\bar{q})\propto q_q^2/Q^4$ for $m_q\ll Q\ll m_Z$ where q_q is the quark's electric charge, which gives $q_u:q_d:q_s:q_c:q_b=4:1:1:4:1$. Using this ratio, though, affects the results at $2Q=29$ GeV minimally.

64% of the $K^{\pm}$ mesons decay into $\mu^{\pm}+\nu_{\mu}$ and then $\mu^{\pm}\rightarrow e^{\pm}+\nu_e+\nu_{\mu}$. Most of the other $K^{\pm}$ decays produce pions. The K_S^0 and K_L^0 mesons predominantly decay into pions and a small number of leptons. On collider timescales, roughly equal numbers of neutrons and protons are produced. Also, almost equal numbers of π^+, π^-, and π^0 are generated. The pions are the dominant precursors of the stable leptons. In general, these remarks apply too for the other center-of-mass energies in our range and the gluon jets. If equal numbers of each pion species are created, the decays given in Eq. (36) alone produce the astrophysically stable particles in the ratio 20% $e^{\pm}$, 20% γ, and 60% $\nu\bar{\nu}$. This ratio is very similar to those produced by the black holes (see Table II), again indicating that the final emission is mainly jet products.

Agreeing with the relative numbers of $e^{\pm}$, γ, and $\nu\bar{\nu}$ produced by the decays in (36), the $\nu\bar{\nu}$ flux maxima in Fig. 4 are approximately 3 times the $e^{\pm}$ maxima while the $e^{\pm}$ maxima are approximately twice the γ maxima. The energies at the $e^{\pm}$ and $\nu\bar{\nu}$ peaks roughly coincide and are about one third to a half the energies at the γ peak. Assuming π^+, π^-, and π^0 have the same initial energy distributions, we can explain this by noting that the π^0 decays into two photons, each with an average energy of half the original π^0 energy. On the other hand, the $\pi^{\pm}$ decays into $\mu^{\pm}+\nu_{\mu}$ and then $\mu^{\pm}\rightarrow e^{\pm}+\nu_e+\nu_{\mu}$, each with an average energy of about one sixth the original $\pi^{\pm}$ energy (for relativistic decays). (For nonrelativistic $\pi^{\pm}$, the $\mu^{\pm}$ products have an average energy of about one fourth the original $\pi^{\pm}$ energy.) Thus the average final $e^{\pm}$ and $\nu\bar{\nu}$ energies should be about one-third to one-half the average photon energy.

The (b) peaks in the power spectra are listed in Table VIII. Recall that the $E\,d\dot{N}/dE$ peak for the jet-produced hadrons is given by Eq. (21) provided the initial quark or gluon energy is $Q\geq 2.4$ GeV, in the case of $p\bar{p}$, and $Q\geq 16.1$ GeV, in the case of $\pi^{\pm}$. If Q is the energy at which the primary $s=\frac{1}{2}$ power peaks, i.e., $Q\simeq 4.53T$, then we have

$$E'_{\rm peak}\simeq\begin{cases}0.34\sqrt{T}\ \text{GeV}, & \pi^{\pm}\ ,\\ 0.89\sqrt{T}\ \text{GeV}, & p\bar{p}\ .\end{cases} \tag{37}$$

The $T=10$–100 GeV $p\bar{p}$ power spectra do indeed peak at $E'_{\rm peak}\simeq(0.6-1.0)\sqrt{T}$ GeV. For $e^{\pm}$, γ, and $\nu\bar{\nu}$, the scaling is less conclusive but $E'_{\rm peak}\simeq(0.05-0.08)\sqrt{T}$ GeV for $e^{\pm}$ and $\nu\bar{\nu}$ and $E'_{\rm peak}\simeq(0.11-0.16)\sqrt{T}$ GeV for γ. Again the average final lepton energy in the $\pi^{\pm}$ decays should be roughly one sixth to one fourth the $\pi^{\pm}$ $E'_{\rm peak}$, i.e., about $0.05-0.09\sqrt{T}$ GeV. If $E'_{\rm peak}$ is roughly equal for π^0 and $\pi^{\pm}$, the photon flux from π^0 decay should peak at about $0.16\sqrt{T}$ GeV. Given the inaccuracy in reading $E'_{\rm peak}$ off the histograms and our neglect here of the details of the decay dynamics, this reasonably explains the peak energies. Because the protons and antiprotons result from decay chains with fewer steps and are also heavier, thus suffering loss momentum smearing, the scaling relation (37) applies more strongly to them.

In the π^0 rest frame, we have $E=m_{\pi^0}/2$ for both of the π^0-decay photons, by momentum conservation. Thus, in the frame where the π^0 velocity is v, the photon energy will lie in the range $m_{\pi^0}/2\rho\leq E\leq\rho m_{\pi^0}/2$ where $\rho=\sqrt{(c+v)/(c-v)}$. The energy where the photon distribution peaks increases but, if most of the final π^0's are nonrelativistic, dN_{γ}/dE should still peak at about $m_{\pi^0}/2$. The exact form of the π^0 distribution in the jets should give the low energy $E^{0.5}$ to E^1 slopes seen below the γ flux peaks in Fig. 4, and the corresponding E^1 to E^2 slopes in the power. In contrast, the primary $s=1$ flux has an E^3 slope at low energies and the primary quark flux has an E^2 slope (see Sec. III C).

In the rest frame of the decaying $\pi^{\pm}$, the muon kinetic energy is $E_{\mu}=(m_{\pi}-m_{\mu})^2/2m_{\pi}\simeq 4.12$ MeV, by energy and momentum conservation. The ν_{μ} energy is $E_{\nu_{\mu}}=(m_{\pi}^2-m_{\mu}^2)/2m_{\pi}\simeq 29.8$ MeV. The final $e^{\pm}$, ν_e, and ν_{μ} distributions, shown in Fig. 7, are given by Eqs. (38) (see below), together with the ν_{μ} at 29.8 MeV. In the $\pi^{\pm}$ rest frame, $dn_{e^{\pm}}/dE$ and dn_{ν_e}/dE peak at $E_{e^{\pm}}\simeq 56$ MeV and $E_{\nu_e}\simeq 37$ MeV, respectively, and have slopes of E^2 below the peaks. Since most jet pions are nonrelativistic, we would expect the final lepton flux to peak close to these energies and have the same low-energy slopes, were not the slopes masked by the neutron β decay. The lepton power, as shown in Fig. 5, does vary as E^2 to E^3 between the (a) and (b) peaks.

From Figs. 4 and 5 and Tables VII and VIII, we can

TABLE XIV. The errors in plotting $d\dot{N}/dE$ and $E\,d\dot{N}/dE$ with E in GeV for $T=0.1$ GeV, Fig. 12 cases (i) and (ii). The errors at all other energies are less than 10%.

	$e^{\pm}$	γ	$\nu\bar{\nu}$
Flux	50% for $E<0.01$ 25% for $E>0.2$	50% for $E<0.05$ 25% for $E>0.2$	30% for $E<0.01$ 25% for $E>0.2$
Power	30% for $E<0.01$ 30% for $E>0.2$	30% for $E<0.04$ 50% for $E>0.2$	25% for $E<0.006$ 50% for $E>0.2$

also see that the pion decay flux and power peaks (b) increase by 3 orders of magnitude between $T=0.3-100$ GeV. In contrast, the peak primary flux remains constant per particle degree of freedom and the peak primary power is proportional to T. The energies at the $d\dot{N}/dE$ peaks do not scale with T but remain at $E_{\text{peak}}\simeq 60-70$ MeV for γ and $E_{\text{peak}}\simeq 20-35$ MeV for $e^{\pm}$ and $\nu\bar{\nu}$; E_{peak} increases four-fold between $T=1-100$ GeV for $p\bar{p}$. For the photons, which come mainly from the nonrelativistic π^0's, this agrees with our comments above on π^0 decay. The $e^{\pm}$ and $\nu\bar{\nu}$ peaks, however, are distorted by the low-energy products from other decays, most noticeably the neutron decay: the $T=10-100$ GeV $e^{\pm}$ flux peaks are distorted below $E\simeq 100$ MeV by the β decay so that the $\pi^{\pm}$ decay now appears as a plateau at 20–30 MeV. (The total $e^{\pm}$ β-decay energy, however, is so small that it only produces a bump on the corresponding power spectra.) Since $E_{\text{peak}}\simeq\sqrt{\mu Q/2}e^{-A(\ln Q/\Lambda_{\text{QH}})^{3/2}}$, in the case of hadron flux, and μ is much greater for $p\bar{p}$ than for $\pi^{\pm}$, we do expect E_{peak} to increase more strongly with Q for $p\bar{p}$ than for $\pi^{\pm}$. After looking at Table VIII, we conclude that the exponential term holds the E_{peak} in the π^0 flux roughly constant for $T=0.3-100$ GeV, while there may be a slight decrease for $\pi^{\pm}$. The fluxes also indicate that most of the decaying pions are nonrelativistic—the pions result from long fragmentation sequences which tend toward the lightest, stable particles.

Above the peaks, the jet pion distributions produce the E^{-1} slope (see Sec. III C) which can be seen to some degree on all γ, $e^{\pm}$, and $\nu\bar{\nu}$ flux spectra between $E\simeq 0.1$ GeV $-T$. Above $E\simeq T$, either side of the direct emission peaks (c), all spectra have the exponential tail in the Hawking distribution of initial jet energies.

4. *Comparison of quark and gluon jets*

The average multiplicity per gluon jet is greater than that per quark jet due to the greater color charge of the gluon. This leads to increased gluon bremsstrahlung in the fragmentation process and a greater number of decay steps. Thus, by energy conservation, the average energy of the final particles is less for the gluon jets. The decays of quark and gluon jets with initial energies of $Q=40$ GeV are presented in Fig. 8 and Tables IX and X. (Again, since the program only stores rest masses to 1 MeV, the spectra may be unreliable below 1 MeV.) Because $Q<m_t$, the quark jet spectra are averaged over five flavors giving equal weight to each. The quark and gluon spectra are strikingly similar to the $T=10$ GeV spectra, even though Fig. 10 does not include the Hawking distribution. This is because the jet spectra, for the most part, determine the shape of the emission spectra since the jet spectra fall off less quickly away from the peak than does the Q distribution. The $e^{\pm}$ and $\nu\bar{\nu}$ spectra from the quark and the gluon jets both have the low-energy neutron β-decay peaks. The main peaks on the $e^{\pm}$, γ, and $\nu\bar{\nu}$ spectra, between about 0.01–1 GeV, come from jet pion decay. The upper cutoffs are slightly less steep than the exponential cutoff in the emission and the small high-energy direct peaks (c) are also noticeably missing. The E^{-1} slope which we anticipated in Sec. III C can be seen most clearly on the quark $p\bar{p}$ flux between about 1 and 10

TABLE XV. Distributions of total flux and power, multiplicities and average kinetic energies for $T=0.02$ GeV: case (i) with primary pion emission. No $p\bar{p}$ are emitted.

$T=0.02$ GeV	$e^{\pm}$	γ	$\nu\bar{\nu}$
Flux	35.76% (±0.85%)	5.44% (±0.44%)	58.80% (±1.75%)
		$\dot{N}_{\text{tot}}=2.66(\pm 0.05)\times 10^{21}$ GeV^{-1} sec^{-1}	
Power	35.97% (±1.35%)	7.68% (±0.78%)	56.36% (±2.51%)
		$P_{\text{tot}}=2.03(\pm 0.06)\times 10^{20}$ sec^{-1}	
Peak flux (GeV^{-1} sec^{-1})	$1.01(\pm 0.05)\times 10^{22}$	$1.48(\pm 0.07)\times 10^{21}$	$1.52(\pm 0.08)\times 10^{22}$
at E_{peak} (GeV)	0.066 (±0.006)	0.107 (±0.007)	0.079 (±0.007)
Peak power (sec^{-1})	$8.0(\pm 0.4)\times 10^{20}$	$1.66(\pm 0.08)\times 10^{20}$	$1.30(\pm 0.07)\times 10^{21}$
at E'_{peak} (GeV)	0.087 (±0.004)	0.120 (±0.005)	0.085 (±0.006)
Multiplicities	0.43 (±0.02)	0.07 (±0.02)	0.71 (±0.01)
$\bar{E}$ (GeV)	0.076 (±0.001)	0.107 (±0.001)	0.073 (±0.001)

GeV, with a corresponding plateau in the power. The slope of about $E^{0.5}$ to E^{1} in the photon flux at $E \lesssim 0.01$ GeV comes from the low-energy tail in the π^0 decay.

Below $E \lesssim 1$ GeV for $e^{\pm}$, γ and $\nu\bar{\nu}$ and $E \lesssim 3$ GeV for $p\bar{p}$, the flux and power per gluon jet are roughly twice the flux and power per quark jet. Since the total energy in a jet must be conserved, the quark spectra dominate at higher energies. Overall, the shapes of the $e^{\pm}$, γ, and $\nu\bar{\nu}$ spectra differ little between the two types of jets. Looking at Table X, we can see, though, that more of the quark products must be pion decays since pion decay alone would produce the ratio 0% $p\bar{p}$, 20% $e^{\pm}$, 20% γ, and 60% $\nu\bar{\nu}$. For each species, the average multiplicities per initial gluon are (50–65)% greater than that per quark: 51.39(±0.16) final states are produced per quark and 78.9(±0.4) per gluon. Again by energy conservation, the final particles in the gluon jets have a smaller average energy.

To obtain the black-hole emission spectra, the quark and gluon decay spectra are convolved with the Hawking distribution and weighted by the initial particle's spin and degrees of freedom. For a $T=10$ GeV hole emitting five flavors, 87.35(±0.38%) of the jet products [or 86.02(±0.36%) of the total flux] and 90.16(±0.91%) of the jet energy [or 69.8(±1.1%) of the total power] comes from quark, as opposed to gluon, jets.

5. *High-energy primary emission peaks*

The flux and power peaks (c) occur at $E \simeq 4T$ for $e^{\pm}$ and $\nu\bar{\nu}$ and $E \simeq 6T$ for γ. There is no direct $p\bar{p}$ peak (since all $p\bar{p}$ are jet products). The primary $e^{\pm}$, γ, and $\nu\bar{\nu}$ emission is superimposed on the exponential tail of the jet emission. Thus, while the heights of the peaks (c) are in the expected order for direct emission, i.e., $\gamma < e^{\pm} < \nu\bar{\nu}$, they also reflect a small jet contribution at these energies. The flux peaks (c) are 2 orders of the magnitude less than the (b) peaks for $T=0.3$ GeV and 5 orders of magnitude less for $T=100$ GeV. The power peaks (b) are ~ 1.5 orders of magnitude greater for $T=0.3$ GeV and 2 orders of magnitude greater for $T=100$ GeV. As we earlier noted, the peak primary flux remains constant at 2.35×10^{21} GeV sec^{-1} per $s=\frac{1}{2}$ helicity state [see Eq. (8)] and the peak primary power is proportional to T.

6. *Primary muon and tau decays*

The decays of the directly emitted $\mu^{\pm}$ and $\tau^{\pm}$ are also present in the final spectra. The muons decay via $\mu^{\pm} \rightarrow e^{\pm} + \nu_e + \nu_\mu$. In the rest frame of the muon, the differential probability that a muon produces an electron of energy E_e and an $\bar{\nu}_e$ of energy E_{ν_e} is proportional to[32] $d\Pi \propto m_\mu E_{\nu_e}(m_\mu - 2E_{\nu_e})dE_e dE_{\nu_e}$ with $(m_\mu/2)-E_e \le E_{\nu_e} \le m_\mu/2$ and $0 \le E_e \le m_\mu/2$. (Here we have neglected the electron rest mass $m_e \simeq m_\mu/200$.) Thus, Lorentz transforming into the frame where the muon's kinetic energy is $E_\mu = (\gamma-1)m_\mu$, we have

$$\frac{dn}{dE_e} \propto m_\mu^2 E_e^2 \gamma \left[\gamma(4-\gamma^{-2}) - \frac{4E_e}{m_\mu}\right],$$
$$\frac{dn}{dE_{\nu_e}} \propto m_\mu^2 E_{\nu_e}^2 \gamma \left[\frac{\gamma}{3}(4-\gamma^{-2}) - \frac{2E_{\nu_e}}{m_\mu}\right], \qquad (38)$$
$$\frac{dn}{dE_{\nu_\mu}} \propto m_\mu^2 E_{\nu_\mu}^2 \gamma \left[\gamma(4-\gamma^{-2}) - \frac{4E_{\nu_\mu}}{m_\mu}\right]$$

TABLE XVI. Distributions of total flux and power, multiplicities and average kinetic energies for $T=0.02$ GeV: case (ii) without primary pions. No $p\bar{p}$ are emitted.

$T=0.02$ GeV	$e^{\pm}$	γ	$\nu\bar{\nu}$
Flux	36.79% (±0.88%)	4.46% (±0.43%)	58.75% (±1.19%)
		$\dot{N}_{\rm tot}=2.53(\pm0.05)\times10^{21}$ GeV^{-1} sec^{-1}	
Power	36.78% (±1.90%)	6.54% (±0.79%)	56.68% (±2.75%)
		$P_{\rm tot}=1.93(\pm0.06)\times10^{20}$ sec^{-1}	
Peak flux (GeV^{-1} sec^{-1})	9.5(±2) $\times10^{21}$	1.23(±0.25) $\times10^{21}$	1.42(±0.3) $\times10^{22}$
at $E_{\rm peak}$ (GeV)	0.068 (±0.005)	0.115 (±0.005)	0.072 (±0.006)
Peak power (sec^{-1})	8(±2) $\times10^{20}$	1.5(±0.3) $\times10^{20}$	1.20(±0.24) $\times10^{21}$
at $E'_{\rm peak}$ (GeV)	0.087 (±0.012)	0.123 (±0.008)	0.091 (±0.004)
Multiplicities	0.42 (±0.02)	0.05 (±0.02)	0.69 (±0.01)
$\bar{E}$ (GeV)	0.075 (±0.001)	0.112 (±0.001)	0.074 (±0.001)

with the constraints that $E_e, E_{\nu_\mu} \leq \gamma m_\mu [1+(1-\gamma^{-2})^{1/2}]/2$ and $E_{\nu_e} \leq m_\mu \gamma (4-\gamma^{-2})/6$. Noting that $\int dn_{e,\nu_e,\nu_\mu} = 1$, the normalizing factors in (38) are then

$$k_e^{-1} = \frac{m_\mu^5 \gamma^5}{48}[1+(1-\gamma^{-2})^{1/2}]^3 \times [5-2\gamma^{-2}-3(1-\gamma^{-2})^{1/2}] = k_{\nu_\mu}^{-1} ,$$
$$k_{\nu_e}^{-1} = \frac{m_\mu^5 \gamma^5}{7776}(4-\gamma^{-2})^4 . \quad (39)$$

The spectra peak at $E_e = E_{\nu_\mu} = \gamma m_\mu (4-\gamma^{-2})/6$ and $E_{\nu_e} = \gamma m_\mu (4-\gamma^{-2})/9$ (see Fig. 9). Below the peaks, both the spectra in the muon rest frame and the Lorentz-transformed spectra have E^2 slopes. All the Lorentz-transformed spectra peak at about the total muon energy.

The tau leptons fragment into hadrons and leptons. Our program decays a $\tau^+\tau^-$ pair into leptons or leptons plus a $q\bar{q}$ pair which is then treated as a final hadronic cluster of the same mass. The spectra of final states are approximately those seen in the laboratory, although details of their generation may not be too reliable. Figure 10 shows the $\tau^\pm$ decay products from a $T=10$ GeV black hole. The average number of decay products per emitted $\tau^\pm$ are 0 $p\bar{p}$, $1.53(\pm 0.02)e^\pm$, $1.42(\pm 0.02)\gamma$, and $5.17(\pm 0.02)\nu\bar{\nu}$ for $n=1000$ events. The contributions to the $0.1 \lesssim E \lesssim 1$ GeV emission spectra from the primary $\tau^\pm$ and $\mu^\pm$, however, are negligible compared with the jet emission. The high-energy $\tau^\pm$ and $\mu^\pm$ decay products and the jet component smear out the spectra just below the direct $e^\pm$ and $\nu\bar{\nu}$ peaks (c). While the jet products far outnumber the decay products of the primary leptons, the combined nonjet emission constitutes about 20% of the total power.

B. The $T=0.1$ GeV emission

To check the Monte Carlo code at low energies, we ran two $T=0.1$ GeV programs: (i) with directly emitted pions if $0.1 < Q < 0.3$ GeV and QCD jets above 0.3 GeV; and (ii) without primary pions which attempts to emit jets at all energies. The results are shown in Fig. 11 and Tables XI–XIII. The $e^\pm$ and $\nu\bar{\nu}$ flux peak at 20–60 MeV. The photon flux peaks at 50–100 MeV. At low energies, the lepton fluxes have the E^2 slopes associated with the primary $s=\frac{1}{2}$ emission and the $\pi^\pm$ decay; the photon flux has the E^3 slope associated with the $s=1$ emission. The bumps on all spectra at 0.3–0.6 GeV are the primary $e^\pm$, γ, and $\nu\bar{\nu}$. The spectra, however, are mainly pion products from the q_u and q_d jets. We wanted to check this: all reasonable jet codes should produce only pions and leptons (on collider timescales) as the initial quark energy approaches $m_{u,d}$.

The spectra differ substantially from the $T=0.3$ GeV spectra: there is a negligible neutron contribution and less than 10^{-2} fewer $p\bar{p}$ than for $T=0.3$ GeV—insufficient to plot. The energies where the flux peaks in cases (i) and (ii) roughly coincide. They also roughly equal those of the $T=0.3$–100 GeV pion decay peaks (b). The power peaks at slightly higher energies in case (ii) than in case (i). The peak $e^\pm$, γ, and $\nu\bar{\nu}$ flux and power in case (ii) are also about (10–20)% smaller. Using the results of Sec. III C, the power should peak at $E \simeq Q_c/12 \simeq 0.125$ GeV for $e^\pm$ and $\nu\bar{\nu}$ and at $E \simeq Q_c/4 \simeq 0.375$ GeV for γ, if $Q_c \simeq 1.5$ GeV. The $e^\pm$ and $\nu\bar{\nu}$ peaks agree reasonably well with this. The photon power peaks at a somewhat lower energy, perhaps due to a different effective Q_c for π^0 (which is likely since more of the π^0 than π^- or π^+ result from η decay). The ratio of the peak fluxes suggests that the peaks come from roughly equal numbers of π^+, π^-, and π^0 created in the $q_{u,d}$ jets. Since[43] the number of external lines in the diagrams describing the jet decay (in effect a measure of the number of decay steps between the initially emitted quark or gluon and the final states) and the length of the lines increase with Q, the pion energy distributions in the low-energy jets should more closely resemble those of the initial quarks. This is most noticeable in the shape of the photon spectra which do not include $\mu^\pm$ decay.

The fraction of the total flux and power carried by each species and the multiplicities differ little between the two cases. The $p\bar{p}$ fraction should be slightly smaller with primary pions but this is beyond the accuracy of the program. Considering the fractions and multiplicities produced if $e^\pm$, γ, $\nu\bar{\nu}$, and $\mu^\pm$ were the only direct emission, both cases show a sizable low-energy $q_{u,d}$ jet contribution. Roughly one-half of the photons must be jet products. For case (i), $66.2(\pm 1.5\%)$ of the flux and $53.6(\pm 3.1\%)$ of the power and for case (ii), $74.5(\pm 1.4\%)$ of the flux and $55.4(\pm 3.0\%)$ of the power, are jet products. The direct pions increase the total flux by about $14.9(\pm 1.1\%)$ and the power by about $8.2(\pm 0.4\%)$. The average kinetic energies of the final states in both cases are well below the average energy of the primary particles. Since $T \lesssim 0.3$ GeV and jet evaporation is decreased, the emission no longer satisfies the parametrizations (29)–(34): the flux is overestimated by a factor of 5 and the power by a factor of 2.

The differences between the two cases are upper estimates for the effect of the uncertainty in any particle model in the regime between primary pion emission (which we know must occur at $Q \simeq m_\pi \simeq 0.14$ GeV) and primary quark and gluon emission (at $Q \gtrsim 0.3$ GeV). These errors, however, have little effect on the total lifetime emission from a black hole or the emission from a PBH background.

C. The $T=0.02$ GeV emission

A $T=0.02$ GeV black hole has a mass of $M = 5.29 \times 10^{14}$ g $\simeq M_*$ and a lifetime close to that of the Universe. M_* holes would be the most numerous today if primordial black holes formed from a Zel'dovich-Harrison spectrum of initial inhomogeneities. The results are shown in Fig. 12 and Tables XII–XVI. In case (i), pions are directly emitted if $m_\pi < Q < 0.3$ GeV and quarks and gluons are emitted if $Q > 0.3$ GeV; the Q distribution is also cut off at $2QT = 0.4$ GeV, rather than $10T = 0.2$ GeV, so that the code can attempt to generate jets. Case (ii) produces no primary pions and attempts jet emission if $Q > 100$ MeV.

At low energies, the $e^{\pm}$ and $\nu\bar{\nu}$ flux have the E^2 slope associated with the direct $s=\frac{1}{2}$ emission and the nonrelativistic $\pi^{\pm}$ and $\mu^{\pm}$ decays. There is also, in case (i), a plateau in the lepton spectra at about 25–80 MeV and, in case (ii), a peak at about 50–80 MeV. Above the peaks, all spectra fall off exponentially. The photon flux has a low-energy E^3 slope and, in case (i), a plateau at $E\simeq 70-120$ MeV and, in case (ii), a peak at $E\simeq 100-120$ MeV, followed by the exponential tail of the Hawking distribution. To within the accuracy of the program, no jets (or $p\bar{p}$) are generated: since the Q distribution falls off steeply above $5T$, less than 1% of the primary particles have $Q>0.2$ GeV. The primary emission here includes $e^{\pm}$, γ, $\nu\bar{\nu}$, $\mu^{\pm}$, and in case (i), π^0 and $\pi^{\pm}$. The primary $s=\frac{1}{2}$ flux and power peak just below $m_{\mu}=0.1057$ GeV. The low- and high-energy $e^{\pm}$, γ, and $\nu\bar{\nu}$ slopes, the multiplicities, the peak in case (ii), and the upper half of the plateaus in case (i), predominantly come from the primary $e^{\pm}$, γ, and $\nu\bar{\nu}$. The ratio of the peak flux is about $e^{\pm}:\gamma:\nu\bar{\nu}\simeq 2:0.3:3.0$, as expected from Eq. (8). The lower half of the plateaus in case (i) are associated with the decay of the primary nonrelativistic $\pi^{\pm}$ and π^0. The ratio of the plateaus imply that the muons and the primary $e^{\pm}$ and $\nu\bar{\nu}$ also contribute somewhat to the spectra here. The average kinetic energies of the final particles are close to, but slightly less than, the peak energies in the primary power, due to the small muon and pion contributions. Since our programs use the relativistic muon and pion absorption coefficients Γ_s, the muon and pion contributions may be overestimated by up to a factor of 2 at this temperature. The parametrizations (30)–(32) overestimate the total $T=0.02$ GeV flux and power by about an order of magnitude.

Again the difference between our two cases is an upper estimate of the effect of error in any particle model at $0.1<Q<0.3$ GeV since some primary pions should be emitted at these Q. The difference in $N_{\rm tot}$ and $P_{\rm tot}$, as displayed in Tables XV and XVI, and the heights of the spectra (except the plateaus) is less than a few percent. Astronomical observations of the total flux and power from a $T\simeq 0.02$ GeV black hole may indicate the correct particle model if T or M is accurately known. The spectral shape, in particular the pion decay plateaus, may give more information on the correct particle model.

D. Effects of additional particle species

Although our program includes the top quark, this particle has yet to be seen. Its existence is required by quark-lepton symmetry in the standard model. The model, however, cannot predict m_t but current measurements imply[44] 89 GeV $\lesssim m_t \lesssim$ 250 GeV. Since the primary $T=50,100$ GeV emission peaks above 200 GeV and we have already included m_t decays in these programs, only our $T\simeq 10$ GeV spectra could be significantly affected by the true m_t. Since the expected q_t jets resemble the q_b jets and the multiplicities are increased by a factor $\lesssim 2$, the $T\simeq 10$ GeV spectra at all E could change by at most a factor of about 3.

A fourth lepton-quark family at high energies, adding another 28 $s=\frac{1}{2}$ degrees of freedom, would increase the net flux and power of fundamental particles by about a third. The shape of the spectra, though, may be significantly affected since the multiplicities will increase with further flavors, as well as higher initial Q.

The $T=50,100$ GeV black holes will also emit $W^{\pm}$ and Z^0 particles where $m_{W^{\pm}}=81.8(\pm 1.5)$ GeV and $m_Z=92.6(\pm 1.7)$ GeV. The decays include $W^{\pm}\rightarrow e^{\pm}+\nu_e,\mu^{\pm}+\nu_{\mu}$, $q_1+\bar{q}_2$ and $Z\rightarrow e^+ + e^-,\mu^+ + \mu^-,q+\bar{q}$. Since the average lepton energy in the purely leptonic decays is at least $m_{W^{\pm}}/2$ or $m_{Z^0}/2$, the lepton emission should be enhanced above $E\simeq 40$ GeV. Because there are only two or three helicity states for each W^-, W^+, and Z^0 particle, depending on Q, and $\dot{N}$ per $s=1$ helicity state is about one third that per $s=\frac{1}{2}$ state, the contribution from the $W^{\pm}$ and Z^0 leptonic decays is at most one half or three quarters that of a directly emitted lepton. When $W^{\pm}$ decays into two quark jets, the initial quark and antiquark have different flavors to preserve a net electric charge. The jets, though, are very similar to the single flavor Z^0 quark-antiquark jets. Since BIGWIG uses $e^+ + e^- \rightarrow Z^0 \rightarrow q+\bar{q}$ for $2Q\gtrsim m_Z$, the Z^0 and $W^{\pm}$ jets resemble two primary quark (or antiquark) jets each with an initial energy half the Z^0, $W^{\pm}$ energy. However, since each quark flavor has 12 degrees of freedom, the $W^{\pm}$ and Z^0 decays are swamped by the directly emitted quark jets. In summary, the $W^{\pm}$ and Z^0 emission has little effect on the overall spectra, the rate of mass loss dM/dt or the lifetime of a black hole.

The consequences of the emission of $s=0$ Higgs bosons, not yet seen experimentally, depend strongly on the unknown Higgs-boson mass. For example, if $m_{\rm H}\simeq 10-80$ GeV then the dominant decay $H\rightarrow q_b+\overline{q_b}$ will increase the q_b jet contribution; if $m_{\rm H}\simeq 80-160$ GeV, the dominant mode $H\rightarrow q_t+\overline{q_t}$ will increase the q_t jet contribution; and if $m_{\rm H}\gtrsim 160$ GeV, the decays $H\rightarrow q_t+\overline{q_t}$, $H\rightarrow W^+ + W^-$, and $H\rightarrow Z^0+\overline{Z^0}$ increase the lepton numbers and the q_t jet contribution. For energies around $m_{W,Z}$, there is one Higgs mode. For $m_{\rm H}\simeq 10-160$ GeV, the "effective" number of q_b and q_t states increases from the 24 of standard QCD to 29.5 [see Eq. (10)]. Each H jet, however, will have an initial energy of half that of the directly emitted quarks. Since the q_b and q_t jet multiplicities are much greater than those of the lower-mass quarks, this will increase the final flux by about up to 50%, depending on $m_{\rm H}$, m_t, and T. If $m_{\rm H}\gtrsim 160$ GeV, the increase in the final flux due to the extra lepton and q_t decay will depend on $m_{\rm H}$ and the branching ratio for these H decays.

On a more speculative note, let us consider the $N=1$ supersymmetry model. Each established particle has a supersymmetric partner in this model—an $s=\frac{1}{2}$ particle has an $s=0$ superpartner; an $s=1$ particle, an $s=\frac{1}{2}$ superpartner. The decays $\tilde{q}\rightarrow\tilde{\gamma}+q$ and $\tilde{g}\rightarrow\tilde{\gamma}+q+\bar{q}$ increase the effective number of quark states from the 72 of QCD to 301, with a corresponding increase in the final jet contribution. The direct supersymmetric lepton decays $\tilde{l}\rightarrow\tilde{\gamma}+l$ will produce bumps on the final emission spectra at roughly one-half the peak primary $s=0$ energy. Since a black hole is more like to emit an $s=0$ rather than a $s=\frac{1}{2}$ particle, these contributions will dominate the

directly emitted leptons. Although we cannot proceed in detail (since neither the masses or existence of supersymmetric particles are known), we can say that the shapes of all final spectra will resemble those for the standard model, since again most of the spectra will derive from jet decays.

In general, astrophysical observations of the evaporation and lifetimes of high-temperature ($T \gtrsim 10$ GeV) black holes will give an indication of the number of fundamental particles in nature. Further flavors or new interactions could have dramatic effects at the temperatures that we have considered. For example, the $E_8 \times E_{8'}$ superstring model, in which the Glashow-Weinberg-Salam particles in one E_8 are complemented by "shadow" particles in the other $E_{8'}$ sector, will double the evaporation rates and halve the lifetimes[49] for $T = 0.3-100$ GeV. On the other hand, an increase in the flux and power of just a factor of 2 may be difficult to observe. If shadow particles remain massless at low energies, however, they will dominate the $T = 0.02$ GeV emission.

VI. CONCLUSIONS

In this paper we have calculated the emission from $T = 0.02$ to 100 GeV black holes, including for the first time the emission of quark and gluon jets. The emission spectra are substantially different from those predicted without the jets. Most of the particles have energies well below the peak energy of the primary emission. The $e^{\pm}$, γ, and $\nu\bar{\nu}$ $T = 0.1-100$ GeV spectra are dominated by the decays of the jet pions. All emitted protons and antiprotons are jet products. The total number of particles produced by a $T = 0.3-100$ GeV black hole per unit time is proportional to $T^{1.6\pm0.1}$ and not T. Correspondingly, the average energy of the emission increases more weakly than T. Since the $T \gtrsim 100$ GeV emission should also be dominated by particle decays, and not the nondecaying primary emission, the behavior above $T \simeq 100$ GeV should be similar. This will affect previous calculations of astrophysical scenarios which have invoked a total flux and average energy proportional to T (see Ref. 8). The calculation of the lifetime of an $M \lesssim M_*$ black hole will also depend[11] on the emission of particles with rest masses $\gtrsim 100$ MeV. This work forms the basis for the calculation of the particle backgrounds produced by evaporating black holes over the lifetime of the Universe.[8,12]

ACKNOWLEDGMENTS

The authors would like to thank Bernard Carr for discussion and guidance of this work, Don Page for kindly supplying the numerically generated absorption coefficient, and the Fermilab Astrophysics and Theory Groups for hospitality and computer time. J.H.M. is also indebted to Bill Press at the Harvard-Smithsonian Center for Astrophysics where part of the work was written.

---

*Present address: Code 665, NASA/Goddard Space Flight Center, Greenbelt, MD 20771.

[1]S. W. Hawking, Nature (London) **248**, 30 (1974).
[2]S. W. Hawking, Commun. Math. Phys. **43**, 199 (1975).
[3]B. J. Carr, Astrophys. J. **206**, 8 (1976).
[4]D. N. Page and S. W. Hawking, Astrophys. J. **206**, 1 (1976).
[5]B. J. Carr, in *Observational and Theoretical Aspects of Relativistic Astrophysics and Cosmology,* edited by J. L. Sanz and L. J. Goicoechea (World Scientific, Singapore, 1985), p. 1.
[6]D. N. Page, Phys. Rev. D **13**, 198 (1976).
[7]B. J. Carr, Astrophys. J. **201**, 1 (1975).
[8]J. H. MacGibbon and B. J. Carr, Astrophys. J. (to be published).
[9]J. H. MacGibbon, Nature (London) **329**, 308 (1987).
[10]M. S. Turner, Nature (London) **297**, 379 (1982).
[11]J. H. MacGibbon (unpublished).
[12]J. H. MacGibbon (unpublished).
[13]S. W. Hawking, Sci. Am. **236**, 34 (1977).
[14]N. D. Birrell and P. C. W. Davies, *Quantum Fields in Curved Space* (Cambridge University Press, Cambridge, England, 1982), p. 263.
[15]M. J. Perry, Phys. Lett. **71B**, 234 (1977).
[16]J. M. Blatt and V. F. Weisskopf, *Theoretical Nuclear Physics* (Wiley, New York, 1952), p. 520.
[17]A. A. Starobinsky and S. M. Churilov, Zh. Eksp. Teor. Fiz. **65**, 3 (1973) [Sov. Phys. JETP **38**, 1 (1974)].
[18]R. P. Kerr, Phys. Rev. Lett. **11**, 237 (1963).
[19]E. T. Newman *et al.*, J. Math. Phys. **6**, 918 (1965).
[20]C. W. Misner, K. S. Thorne, and J. A. Wheeler, *Gravitation* (Freeman, San Francisco, 1973), p. 877.
[21]B. Carter, Phys. Rev. Lett. **33**, 558 (1974).
[22]D. N. Page, Phys. Rev. D **16**, 2402 (1977).
[23]D. N. Page, Phys. Rev. D **14**, 3260 (1976).
[24]D. N. Page (private communication).
[25]T. Elster, J. Phys. A **16**, 989 (1983).
[26]R. D. Simkins, Ph.D. thesis, Pennsylvania State University, 1986.
[27]T. Elster, Phys. Lett. **92A**, 205 (1983).
[28]S. A. Teukolsky and W. H. Press, Astrophys. J. **193**, 443 (1974).
[29]E. P. Wigner and L. Eisenbud, Phys. Rev. **72**, 29 (1947).
[30]Our discussion augments the discussion in J. Oliensis and C. T. Hill, Phys. Lett. **143B**, 92 (1984).
[31]I. G. Moss, Phys. Rev. D **32**, 1333 (1985).
[32]F. Halzen and A. D. Martin, *Quarks and Leptons: An Introductory Course in Modern Particle Physics* (Wiley, New York, 1984).
[33]G. Marchesini and B. R. Webber, Nucl. Phys. **B238**, 1 (1984).
[34]B. R. Webber, Nucl. Phys. **B238**, 492 (1984).
[35]TASSO Collaboration, M. Althoff *et al.*, Z. Phys. C **22**, 307 (1984).
[36]G. Marchesini and B. R. Webber, Nucl. Phys. **B310**, 461 (1988).
[37]A. Petersen *et al.*, Phys. Rev. D **37**, 1 (1988).
[38]F. James, Rep. Prog. Phys. **43**, 1145 (1980).
[39]A. H. Mueller, Nucl. Phys. **B213**, 85 (1983).

[40]C. Hill, Nucl. Phys. **B224**, 490 (1983).

[41]K. H. Mess and B. H. Wiik, in *Gauge Theories in High Energy Physics,* proceedings of the Les Houches Summer School in High Energy Physics, Les Houches, France, 1981, edited by M. K. Gaillard and R. Stora (North-Holland, Amsterdam, 1983), p. 865.

[42]Particle Data Group, Rev. Mod. Phys. **58**, 323 (1986).

[43]W. Furmanski *et al.*, Nucl. Phys. **B155**, 253 (1979).

[44]S. Geer, in Proceedings of the PASCOS-90 Conference, Boston, Massachusetts, 1990 (unpublished).

[45]A. D. Sakharov, Pis'ma Zh. Eksp. Teor. Fiz. **45**, 237 (1987) [JETP Lett. **45**, 295 (1987)].